Instituto Tecnológico y de Estudios Superiores de Monterrey

Campus Monterrey

School of Engineering and Sciences

Process Intensification of Continuous Antisolvent Crystallization using a Coiled Flow Inverter

A thesis presented by

Andrea Georgina Benítez Chapa

Submitted to the

School of Engineering and Sciences

in partial fulfillment of the requirements for the degree of

Master of Science

In

Energetic Engineering

Monterrey Nuevo León, May 15th, 2018

Instituto Tecnológico y de Estudios Superiores de Monterrey

Campus Monterrey

School of Engineering and Sciences

The committee members, hereby, certify that have read the thesis presented by Andrea Georgina Benítez Chapa and that it is fully adequate in scope and quality as a partial requirement for the degree of Master of Science in Energy Engineering

Dr. Alejandro Juan Álvarez Guerra
Tecnológico de Monterrey
School of Engineering and Sciences
Principal Advisor

Dr. Enrique Alfonso López Guajardo
Tecnológico de Monterrey
Committee Member

Dr. Alejandro Montesinos Castellanos
Tecnológico de Monterrey
Committee Member

Tecnológico de Monterrey
18 MAY 2018
Dirección Nacional de Posgrado
Dr. Rubén Morales Menéndez

Dr. Rubén Morales Menéndez
Dean of Graduate Studies
School of Engineering and Sciences

Monterrey Nuevo León, May 15th, 2018

Declaration of Authorship

I, Andrea Georgina Benítez Chapa, declare that this thesis titled, "Process Intensification of Continuous Antisolvent Crystallization using a Coiled Flow Inverter" and the work presented in it are my own. I confirm that:

- This work was done wholly or mainly while in candidature for a research degree at this University.
- Where any part of this thesis has previously been submitted for a degree or any other qualification at this University or any other institution, this has been clearly stated.
- Where I have consulted the published work of others, this is always clearly attributed.
- Where I have quoted from the work of others, the source is always given. With the exception of such quotations, this thesis is entirely my own work.
- I have acknowledged all main sources of help.
- Where the thesis is based on work done by myself jointly with others, I have made clear exactly what was done by others and what I have contributed myself.

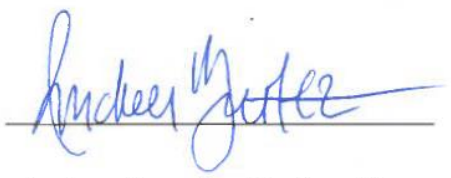

Andrea Georgina Benítez Chapa

Monterrey Nuevo León, May 15th, 2018

To my parents:

Georgina and Alberto.

Acknowledgements

My most sincere gratitude to my thesis advisor Dr. Alejandro Álvarez for his valuable contribution to this work. This thesis would not have been possible without his support and always-inspiring patience and kindness.

Thank you to Dr. K.D.P. Nigam for his involvement in this research, encouragement, advice and most appreciated supervision.

Thank you to Dr. Enrique López for his valuable advice and to both Dr. López and Dr. Alejandro Montesinos for revising and contributing to this thesis project.

Thank you to Professor María Guadalupe Salmerón, with whom I have been working as a Teaching assistant at the Mathematics Department at Tecnologico de Monterrey and to Tecnologico de Monterrey for the economic support provided during my Masters studies.

Special thanks to my mom, my sister Fabiola and my brother Jorge.

Process Intensification of Continuous Antisolvent Crystallization using a Coiled Flow Inverter

by

Andrea Georgina Benítez Chapa

Abstract

The current scenario of the pharmaceutical industry, where final product quality has a fundamental priority, justifies the need for process intensification in order to shift from inefficient conventional batch production to continuous production methods. An alternative to reducing energy consumption in the purification step of pharmaceutical products is antisolvent continuous crystallization, a separation and purification technique that aims to produce particles of controlled size and purity by controlling the antisolvent addition rate, on which crystal birth and growth rates depend.

This work experimentally studies the antisolvent continuous crystallization process of flufenamic acid, an active pharmaceutical ingredient (API), using the coiled flow inverter (CFI) as a novel crystallization device. Two strategies were studied as means to control crystal size distribution in the CFI technology: multistage antisolvent addition and a varied number of the reactor's 90-degree bends. Experimental results show that mean crystal size of the studied API, increased with an increasing number of antisolvent addition points, thus suggesting a growth dominated process. On the other hand, mean crystal size decreased as the number of 90-degree bends increased, suggesting a nucleation dominated process. A narrower crystal size distribution (CSD) was also observed with an increased number of 90-degree bends. When compared to the CFI, mean crystal size and coefficient of variation were, in average, 1.8 and 3.5 times larger for the Kenics type crystallizer, respectively. This can be attributed to the high supersaturation induced by the effective mixing.

Using the Population Balance Equation, as a mathematical model to describe the plug flow crystallization, crystal mass population density was calculated and compared with the obtained experimental data. High regression coefficients were obtained (0.96-0.99), which indicate that

near plug flow behavior was achieved. Consequently, undesired crystallization process phenomena such as agglomeration, dissolution and breakage were successfully avoided, as they can lead to operational problems and a broad CSD.

Process intensification (PI) was measured considering mean crystal size (μm) and coefficient of variation (CV) as product quality indicators. On the other hand, crystallization and pre-expansion temperatures, as well as extraction pressure, were considered as both energy savings and operational safety indicators. Six crystallizers of flufenamic acid were compared (batch, reactor without static mixers, Kenics type crystallizer, Kenics optimized, helical coil and RESS) to a CFI with three 90-degree bends. The CFI was the most intensified technology of all six, with $\mathbf{IF_{total}}$ ranging from 2 (helical coil) to 392 (RESS). For this reason, it can be concluded that the main objective of this thesis, which was to intensify antisolvent crystallization processes, was achieved.

List of Figures

List of Tables

Table of Contents

List of Symbols

Symbol	Definition
A	area, [m^2]
B^0	nucleation rate, [number/m^3 s]
b	nucleation rate order, [dimensionless]
C	solute concentration, [kg/m^3]
C_s	concentration at equilibrium, [kg/m^3]
CV	coefficient of variation
D	diffusion coefficient, [m^2/s]
d_c	coil diameter, [m]
d_{ct}	coil tube diameter, [m]
d_i	internal tube diameter, [m]
d_o	outer tube diameter, [m]
d_p	particle diameter, [m]
E	distribution of the fluid exit times, [dimensionless]
G	growth rate, [m/s]
F_a	intensification factor (after), [dimensionless]
F_b	intensification factor (before), [dimensionless]
g	growth rate order, [dimensionless]
g_c	gravitational constant, [m/s^2]
IF_{total}	total intensification factor, [dimensionless]
k_b	nucleation rate constant, [number/m^3s]
k_g	growth rate constant, [m/s]
k_v	volume shape factor
L	internal coordinate (crystal size), [m]
l	longitude [m]
$\dot{m}$	mass flow rate, [kg/s]
n	population density, [number/m^3 m]
n_{turns}	number of CFI turns, [dimensionless]
n_{seg}	number of CFI segments, [dimensionless]
n_{bends}	number of CFI 90° bends, [dimensionless]
p	pitch, [m]
Q	quantity of solute, [kg/s]
T	time, [s]
t_m	average residence time, [s]
u_x	plug flow velocity, [m/s]
V	volume, [m^3]
W	mass based crystal size distribution
X	external coordinate (axial coordinate), [m]

Greek symbols

x_{cut}	cut-size diameter, [m]
λ	curvature ratio of the helical tube, [dimensionless]
μ	viscosity of the fluid, [kg/m s]
ρ_{sol}	fluid density, [kg/m^3]
ρ_p	particle density, [kg/m^3]
T	residence time, [s]

Dimensionless numbers

De	Dean Number
H	Dimensionless pitch
R_A	CFI performance parameter
Re	Reynolds number
St	Stokes number
T	Torsion parameter

1. Introduction and Motivation

Process intensification is defined as the development of novel process designs aimed at reducing equipment sizes, waste production and capital cost, while improving reaction kinetics, energy efficiency, process safety, and process throughput. Process intensification focuses on the optimal selection and combination of novel and existing state-of-the-art equipment for the efficient use of mass and/or energy (Babi, et al., 2016).

With the aim of achieving improved process efficiency and reduced manufacturing costs, the pharmaceutical industry currently faces the challenge of moving to continuous production processes. Part of the challenge of this transition is to ensure product quality specifications since pharmaceutical products are subjected to limiting particle sizes of a few microns due to their rapid dissolution time and consequent bioavailability (the percentage of absorbed drug compared to its initial dosage quantity, which can be improved by a decreased particle size) (Lonare and Patel, 2013).

Microparticles could be obtained by a top-down or a bottom-up approach. The top-down approach implicates the formation of larger particles which are later milled to a desired final size. Yet this has a number of disadvantages: high-energy input, degradation of bioactive material by excessive local temperatures, and elevated containment costs of fine powders of highly potent drugs together with high costs for frequent reanalysis (Lonare and Patel, 2013; Myerson, 2002; Behr et al., 2004).

An alternative to reducing energy consumption in the purification step of pharmaceutical products is antisolvent continuous crystallization, a “bottom-up” approach. Antisolvent crystallization is a separation and purification technique that aims to produce particles of controlled size, morphology, crystal structure, and purity by controlling the antisolvent addition rate, on which crystal birth and growth rates depend (Alvarez and Myerson, 2010). This technology is simple, cost effective, and easy to scale-up (Lonare and Patel, 2013). It has the advantage of achieving a steady-state operation after about 4 to 5 residence times after the start-up procedure. In this steady state, process parameters do not change, resulting in a robust process (Behr, et al., 2004).

Crystallization is considered the most important separation and purification method in the pharmaceutical industry. It often serves as the final step in the manufacture of active pharmaceutical ingredients (APIs) since over 90% of the APIs are crystals of small organic molecules (Alvarez and Myerson, 2010). Control of crystal size distribution of pharmaceutical products is critical since it affects downstream operations such as flowability, filtration, segregation phenomena, blending, capsule filling, wettability, hydrophobicity, and tabletability (Besenhard, et al., 2015) as well as the physical and chemical properties of the final product (Alvarez, 2009). Thus, crystal engineering can improve the long-term stability and extend shelf life of crystalline pharmaceuticals (Besenhard, et al., 2017).

The control of solution crystallization processes has been studied since the 1940s, but it was not until the 1990s that it became an active area of research. The commercialization of suitable technologies for crystallization modeling and control, in conjunction with the economic support from both pharmaceutical companies and governments in research programs that develop improved methods for obtaining drug crystals of higher consistency and quality, have contributed to the industry take off (Nagy and Braatz, 2012).

1.1 Description of the project

This work experimentally studies the continuous crystallization process of flufenamic acid, a potent nonsteroidal drug using ethanol as solvent and distilled water as antisolvent. As can be observed in **Figure 1.1,** in an ethanol-water system the solubility (mg/mL) of flufenamic acid decreases as the percentage of water increases. Antisolvent crystallization is a standard procedure used to crystallize APIs, which involves the mixing of two miscible fluids: the solution of API and a component that reduces the solubility of the API in the mixed solvent. As a result, API crystallizes out of the solution.

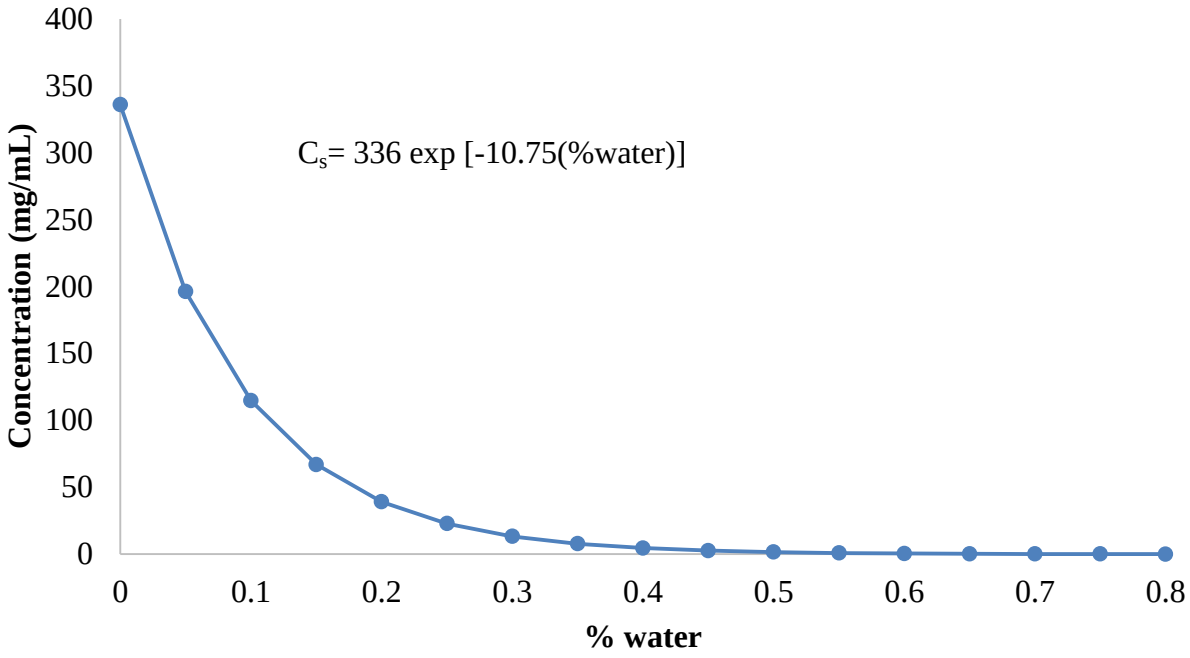

Figure 1.1 Solubility data for Flufenamic Acid in the System Ethanol-Water as a function of Solvent Composition at Room Temperature (Alvarez, 2009).

In antisolvent crystallization, good mixing conditions are essential to avoid creating uneven saturation conditions, which can considerably affect the properties of the product including particle size distribution, morphology, and purity. To guarantee good mixing in antisolvent crystallization processes operated at high supersaturation, different systems have been designed which generate a rapid mixing of solution and antisolvent.

In a helical coil, secondary forces are generated due to the presence of unbalanced centrifugal forces. This results in the formation of symmetrical vortices on the cross-sectional plane of the tube, which effectively augment mixing. The mass transfer limitations of operating at laminar flow conditions, where mixing relies solely on molecular interdiffusion, can be further overcome by creating chaotic advection. Saxena and Nigam (1984) proposed a novel device, the Coiled Flow Inverter (CFI) that inserts equally spaced 90-degree bends in a helical coil. Chaotic trajectories are achieved by multiple flow inversions, resulting in a narrow residence time distribution with near plug flow behavior. A crystallizer operating with near plug flow characteristic is desired since phenomena that affects the final product quality and crystal size distribution, such as agglomeration, breakage or dissolution, are avoided.

This work evaluates the effectiveness of the CFI as a continuous crystallizer. With this purpose, seven different CFIs configurations were constructed. The effect of multiple addition points of antisolvent, as well as the effect of the number of the CFI's 90-degree bends, on the mean crystal size and crystal size distribution (CSD) were experimentally studied and compared with simulated results.

1.2 Justification

Since batch production allows verification of quality of each batch from each process before further processing, regulations have driven pharmaceutical production towards this operation mode. Pharmaceutical processes often contain continuous or semi-continuous processing steps, but the processes are started and stopped to imitate the batch processing (Schaber et al., 2011).

This results in an industry that lacks agility, flexibility, and robustness, which represents a potential public health threat as failures within manufacturing facilities that result in poor product quality can lead to drug shortages (Lee, et al., 2015) or product recalls and harm to patients (Food and Drug Administration, 2017). Moreover, long production times combined with unpredictable demand results in highly fluctuating prices (Jolliffe and Gerogiorgis, 2016).

In this scenario, increased competition from generic manufacturers in addition to steadily increasing research and development costs have brought the pharmaceutical industry to a breaking point (Jolliffe and Gerogiorgis, 2016). Consequently, the pharma industry will have to strengthen its position through cost control. A starting point for creating an efficient supply chain would be the reduction of manufacturing costs, which represent 30% of the total costs in an average pharmaceutical enterprise (Behr, et al., 2004).

Pressure for change not only focuses on the directly visible production costs but also on the indirect costs arising from long manufacturing times, especially in the production of active ingredients. In a study by Macher and Nickerson (2006) it was found that mean cycle time[1] for 36 active pharmaceutical ingredients manufactured in 15 distinct manufacturing facilities from 11 unique pharmaceutical firms was over 29 days.

[1] Average number of days between batch start and those batches either accepted or rejected during the month.

Risk of potential contamination or human error increases with time spent between production steps (Massey, 2016). In the same study by Macher and Nickerson, it was found that mean actual batch yield[2] was 75%.

For these reasons, the Federal and Drug Administration has encouraged drug manufacturers to shift towards continuous production methods (Yu, 2016). Continuous production processes considerably reduce the time required for on-line and in-line process analysis in comparison to batch production (Behr, et al., 2004). Additionally, several authors have demonstrated that continuous processes have lower costs than batch production.

Schaber et al., (2011) compared the costs of batch versus continuous production of 2000 tablets per year of an API. The capital expenditures for continuous production were estimated to be 20 to 76 % lower; while operating expenditures were estimated to be between 40% lower and 9% higher. All continuous production scenarios that incorporate recycling present economical savings. Furthermore, the continuous processes save an average of 61% of the water usage and 21weight percentage of the annual solvent usage compared to batch processing.

Jolliffe and Gerogiorgis (2016) studied and compared continuous versus batch processing of 100 kg/year to 1000 kg/year of two APIs: ibuprofen and artemisinin. Capital expenditure savings of up to 57.0% and 19.6% and corresponding operating expenditure savings of up to 51.6% and 29.3% were determined for ibuprofen and artemisinin, respectively. In addition, the calculated mass of waste generated per unit mass of product was 67% and 20% lower for ibuprofen and artemisinin, respectively.

Some key players in the pharmaceutical industry have already adopted a continuous drug manufacturing method. Eli Lilly and Company, a pharmaceutical company founded in 1876, invested €35 million in a high-tech continuous manufacturing facility in Ireland (Murphy, 2016). One of the projects carried in this facility includes the continuous manufacturing of cancer drug candidate, prexasertib monolactate monohydrate, for clinical trials. In the second continuous flow step of the process, the compound was purified by crystallization. A production of three kilograms of raw material per day was achieved, while maintaining moderate human intervention since the compound is toxic for both healthy and cancerous cells (Extance, 2017).

[2] Ratio of the actual yield to the theoretical yield.

Still, these changes are the exception. Due to the high investments of pharmaceutical industries in the batch production method (to which production licenses are legally tied to according to regulatory legislation), conclusive research must be done to define the applicability limits and benefits of continuous production (Jolliffe and Gerogiorgis, 2016), emphatizing the need for accurate experimental data.

Figure 1.2 shows a general picture of different continuous crystallization methods, as well as several examples of novel continuous antisolvent crystallizers that have been studied in the last decade: Couette-Taylor, continuous oscillatory baffled crystallizer (COBC), sonicated tubular, impinging jets, tee-mixers, and Kenics type crystallizers. Several authors have studied crystallization processes in a CFI (Hohmann, et al., 2018; Hohmann, et al., 2016; Wiedmeyer, et al., 2017), yet literature evaluating this innovative method as crystallization technology is still limited.

In this matter, research must be done to achieve an improved continuous-flow crystallizer design that minimizes operational problems while retaining the advantages of the best previous continuous crystallizers (Jiang, et al., 2014).

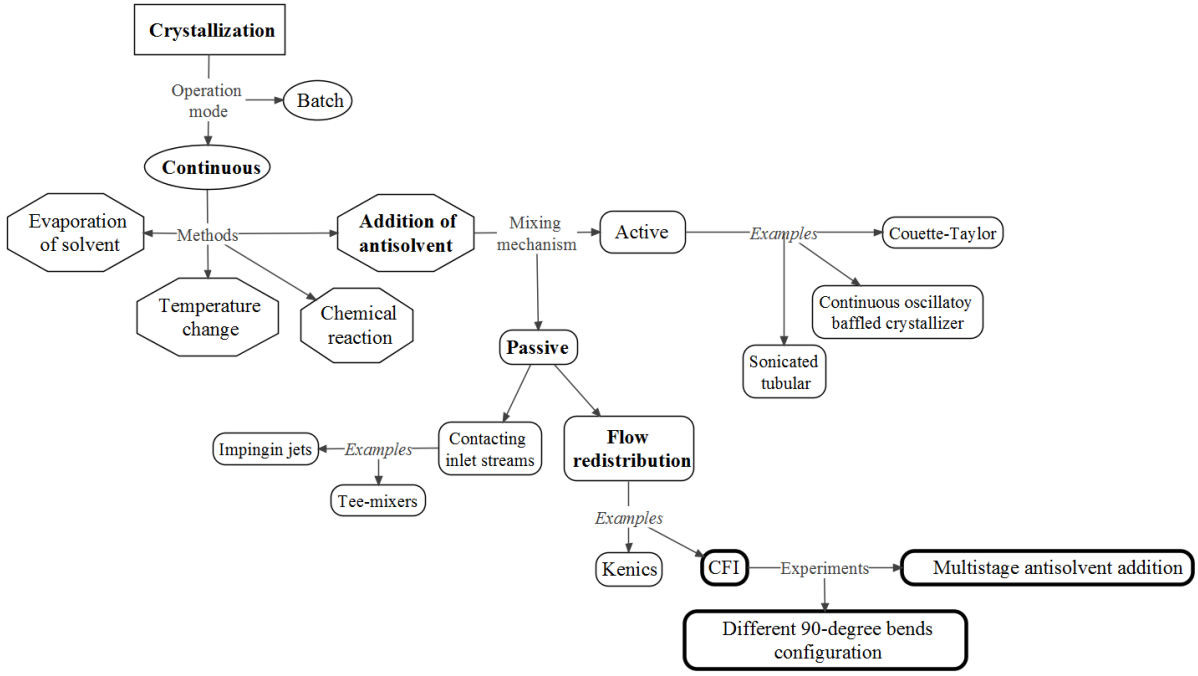

Figure 1.2. Crystallization methods, operation modes and mixing mechanisms**.**

1.3 Objectives

The main objective of this research is to evaluate the CFI technology as an effective API crystallizer. The specific objectives are:

a) Determine the best CFI configuration for antisolvent crystallization.
b) Study product uniformity at the CFI outlet.
c) Evaluate if particle size control is possible in the CFI technology by implementing the following strategies:
    i. Multiple antisolvent injection points.
    ii. Multiple 90-degree inversions.
d) Compare API crystallization process in the CFI to a Kenics type mixer.
e) Compare experimental results to data obtained from mathematical modeling.
f) Draw significant conclusions for crystal behavior in a CFI reactor.
g) Propose a first approximation to process intensification measurement.

This thesis is organized in five chapters. Chapter 1 presents the current scenario of the pharmaceutical industry as technologically stagnant, justifying the need to intensify production processes through continuous operation. Chapter 2 introduces basic crystallization concepts, the methodology for continuous plug flow crystallizers modeling, and the CFI as a novel crystallization device. Chapter 3 covers the experimental work that evaluates the effect of a number of variables (number of points of antisolvent addition and number of 90-degree bends) on the crystal size distribution (CSD). In Chapter 4, the crystallization performance of the CFI is evaluated according to literature's suggested parameters, as well as by the CSD experimental results, which are analyzed and compared to calculated CSDs by the Population Balance Equation for plug flow. Process intensification of the crystallization process is calculated according to a new methodology proposed by literature. Finally, Chapter 5 summarizes the key conclusions of this work and provides recommendations for further research.

2. Theory and State of the Art

This chapter presents a summary of crystallization methods and fundamental terms. Important concepts such as crystal birth and growth are described and later employed for the mathematical modeling of the crystal Population Balance Equation for plug flow behavior. Undesired crystallization phenomena, such as agglomeration and dissolution, are introduced as possible deviations from plug flow. With this in mind, the desired characteristics of a crystallizer are presented and state of the art of active and passive crystallizers is analyzed. After discussing the advantages and drawbacks of these systems, a novel mixing device, the CFI, is described in terms of its working principles and design parameters.

2.1 Basic Crystallization Concepts

A crystal is the most highly organized type of non-living matter. A well-formed solid crystal is, by itself, almost pure (McCabe, et al., 2007). A wide variety of materials are produced in the fine chemical, food, and pharmaceutical industries utilizing crystallization as a separation and purification technique.

Crystallization may be defined as a phase change in which a crystalline product is obtained from a solution. A solution is a mixture of two or more species that form a homogeneous single phase. It typically consists of a solvent, which is a liquid, and a solute, which is a solid. At a given temperature, there is a maximum amount of solute that can dissolve in a given amount of solvent. When this maximum is reached the solution is saturated. A supersaturated solution is formed when the solution concentration exceeds the equilibrium or saturation solute concentration at a given temperature. In order to relieve the supersaturation and move towards equilibrium, the solution crystallizes (Myerson, 2002).

There are four main methods to generate supersaturation. One of them is temperature change, since the solubility of most materials declines with decreasing temperature, cooling is often used to generate supersaturation. However, there are cases of materials whose solubility presents no significant change over the temperature range of interest. In these cases, other methods that create supersaturation must be considered (Myerson, 2002).

The second most commonly used method is evaporation of solvent, in which solvent is removed from the system, thereby increasing the system concentration. If this is done at a constant temperature, eventually the system will become saturated and then supersaturated. After some maximum supersaturation is reached, the system will begin to crystallize.

Another method used to create supersaturation is chemical reaction. In this case, two soluble materials are added together in solutions that react to form a product with low solubility. Since the solubility of the product is soon exceeded, the solution becomes supersaturated and the material crystallizes. Control of the supersaturation in these types of processes is difficult because it requires controlling of the mixing of the reactants and/or the reaction rate (Myerson, 2002). Furthermore, an addition of chemicals may require further separation steps and present additional regulatory and quality control challenges (Besenhard, et al., 2017).

The present work focuses on antisolvent crystallization, a viable crystallization method when evaporation cannot be used because of the lack of reasonable equipment, or because the solvent is not volatile enough and the product is heat sensitive. In this method, another solvent is added to create a mixed solvent system in which the solubility of the solute is greatly decreased. By controlling the rate of the addition, the supersaturation rate is controlled (Myerson, 2002). In antisolvent crystallization, factors controlling crystal size and crystal size distribution include supersaturation, residence time, and addition and mixing of antisolvent. Antisolvent crystallization operated at high supersaturation levels results in crystallized particles of small size (Alvarez & Myerson, 2010).

Crystallization can be carried out on a batch or continuous basis. Batch crystallization drawbacks include low capacity, high requirements of human intervention, and high facility cost. When considering batch processes scale-up, low stirring leads to inhomogeneous crystallization, but high stirring may lead to crystal breakage and broadening of the crystal size distribution (Wiedmeyer, et al., 2017). In batch operation, conditions change with time resulting in crystal characteristics difficult to control and inconsistent from batch to batch, whereas continuous processing has the advantage of enhanced reproducibility of results since all material crystallizes under uniform conditions (Alvarez & Myerson, 2010).

Continuous equipment permits adjusting the operating conditions to get the best results in terms of overall energy usage and product characteristics. Once these conditions have been set, continuous devices can operate reliably for long periods of time.

Continuous operation offers multiple advantages such as improved product quality, cost efficiency, safety, and reduced time-to-market (Hohmann et al., 2016). For these reasons, there is growing interest in applying continuous crystallizers to pharmaceutical process chains. However, this operation mode is still not as universal as batch crystallization in industries. Problems, such as blockage and encrustation, need to be solved by some cost-effective solutions.

2.2 Crystallization Fundamentals

2.2.1 Nucleation

Nucleation is the start of the crystallization process involving the birth of new crystals. Nucleation can be classified as primary, which occurs in the absence of crystalline surface, and secondary, which involves the presence of crystals of the same material acting as attrition agents or seeds. Primary nucleation precedes secondary nucleation (Rohani and Omar, 2017).

Since rapidly occurring crystallization is typically not affected by the presence of solute crystalline material, it does not involve secondary nucleation. Rather, it results from homogeneous or heterogeneous nucleation processes. Homogenous nucleation is the result of pure spontaneous formation of crystal nucleus, while heterogeneous nucleation implicates the formation of nucleus induced by foreign particles or impurities (Myerson, 2002). Secondary nucleation starts at very low supersaturations, while heterogeneous nucleation occurs at less supersaturation compared to the case of homogenous nucleation (Mullin, 2001).

A general theory for the prediction of nucleation rates does not exist, nevertheless, several correlations based in the power law model have been found to explain most of the experimental data satisfactorily (Myerson, 2002). The Classical Nucleation Theory (CNT) is the most common theoretical model used to describe the nucleation process, giving a reasonable prediction of nucleation rates. It is an approximate theory based on the condensation of vapor to liquid, which can be extended to other liquid-solid equilibrium systems from melts and solutions (Karthika, et al., 2016). CNT states that solute molecules collide with each other at a certain frequency due to

Brownian motion, and these collisions lead to the formation of clusters of solute molecules, which continuously aggregate and fall apart until a critical size is reached (the nucleus size) at which become stable and continue to growth spontaneously (Alvarez, 2009). The process of reaching a critical size results in the decrease in the free energy of the system.

The nucleation rate increases with an increase in supersaturation and may be expressed as:

$$B^0 = k_b(C - C_s)^b \tag{2.1}$$

where C is the solute concentration, C_s is the solubility, k_b is the nucleation rate constant and b is the nucleation rate order.

Nucleation will dominate when supersaturation is near or greater than the upper limit of the metastable region. Near the entrance of the crystallizer, the nucleation rate is high and decreases as the supersaturation decreases along the reactor. A great number of crystals are generated in a nucleation driven process, resulting in smaller crystal sizes; however, a nucleation dominated process is generally difficult to control (Alvarez, 2009).

2.2.2 Crystal Growth

As soon as the nuclei reach a critical size, they begin to grow into crystals by the addition and incorporation of units (Myerson, 2002). Crystal growth has been defined as a two-step process. In the first step, solute moves from the bulk of the fluid to the solid surface, while in the second step the crystals arrange themselves into the crystal lattice. From a mass transfer perspective, an increase of the crystal size is caused by the number of growth units joining the surface of the crystal exceeding the number of units leaving it at supersaturated conditions (Alvarez, 2009).

The phenomenon of crystal growth has been attributed to the crystals in a population having a range of internal lattice perfection and/or to surface effects induced by the crystal's growth history (Srisanga, et al., 2015).

The growth rate of crystals due to deposition from the solution on the crystal surface increases with an increase in supersaturation and may be expressed as:

$$G = k_g(C - C_s)^g \tag{2.2}$$

where k_g is the growth rate constant and g is the growth rate order. As supersaturation decreases along the reactor, the growth rate decreases.

Growth and nucleation normally occur simultaneously in industrial crystallizers. However, it has been observed that in some systems there are certain levels of supersaturation where growth will occur and not nucleation. When operating in metastable region, growth will dominate preventing the formation of an excessive number of nuclei. Since the size and purity of the crystal product is defined by the balance between nucleation and growth, local and global saturation ratios are critical (Alvarez, 2009).

2.2.3 Agglomeration

Agglomeration has been defined as a particle size enlargement process by which fine particles are joined in an assembly (Alvarez, 2009). This phenomenon occurs when two particles come close enough for an agglomerative bond to grow. The bond strengthens over time but can be broken by other collisions. Factors that affect agglomeration include surface structure, nature of the agglomerative bond, hydrodynamic effects, effect of supersaturation, and forces involved in aggregation (Rohani & Omar, 2017).

Agglomerates form differently depending on the size. With large crystals, agglomerates get larger by the addition of a single crystal. With small crystals, agglomerates get larger with the addition of smaller agglomerates. Since agglomeration is difficult to predict on a large scale, it can be problematic from an industrial crystallization point of view. Agglomerates can also lead to pharmaceutical stability issues (Rohani and Omar, 2017).

2.2.4 Dissolution

Dissolution occurs when the solution becomes undersaturated. Dissolution can be affected by several crystal characteristics such as shape, size, growth, and form, as well as the chemical nature of both the crystal and the solvent. Dissolution occurs in two phases: (1) the surface reaction and detachment from the surface and (2) the mass transfer of the species from the crystal to the bulk solution through a diffusive layer (Rohani and Omar, 2017).

A flowchart of the processes that make up the birth and death of crystals is shown in **Figure 2.1.**

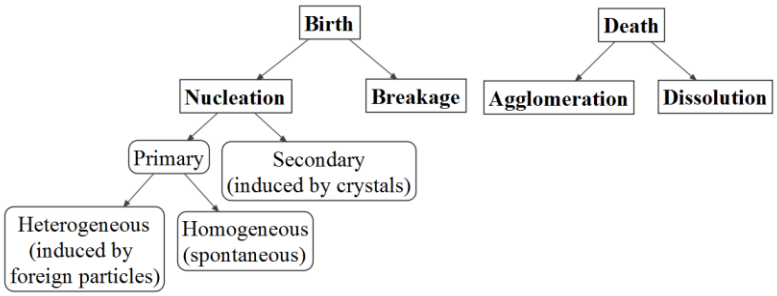

Figure 2.1. Methods of birth and death of crystals (Mullin, 2001; Rohani and Omar, 2017)

2.3 Methodology for Continuous Plug Flow Crystallizers Modeling

A population balance model is defined by the combined phenomenology contained in the displacement of units through their state space and the birth and death processes that terminate existing units and produce new ones. This approach provides a flexible framework for crystallization modeling (Ramkrishna and Mahoney, 2002).

The Population Balance Equation for a plug flow crystallizer at steady state is expressed as:

$$u_x \frac{\partial n}{\partial x} + G \frac{\partial n}{\partial L} = 0 \tag{2.3}$$

where *n*, the population density, is a function of crystal size (L) and distance (x) along the crystallizer, and u_x is the average flow velocity. The first term in equation (2.3) represents the changes in the population density with the position along the tubular reactor. The second term represents the changes in the population density with particle size.

According to Alvarez and Myerson (2010): "*this equation assumes no radial or axial dispersion, growth rate independent of crystal size, and no significant agglomeration, dissolution, or breakage*".

Assuming no seeding or solids present at the entrance, the boundary conditions for equation (2.3) are defined as:

$$n(0, x) = \frac{B^0(x)}{G(x)} \tag{2.4}$$

$$n(L, 0) = 0 \tag{2.5}$$

In addition to the population balance of equation (2.3), mass balance of the system must also be considered. The general form of the mass balance for a plug flow crystallizer is:

$$u_x \frac{dC}{dx} = -3\rho_s k_v G \int L^2 n dL \tag{2.6}$$

where C is the concentration of solute at location x, ρ_s is the density of solid, and k_v is the volume shape factor. Equation (2.6) indicates that for a plug flow crystallizer, the rate of depletion of solute from the solution at any location along the crystallizer must equal the rate at which the mass is gained by the solid.

Solutions of the population equation can be obtained by numerous methods. The Lax-Wendroff scheme, which is a numerical method for the solution of hyperbolic partial differential equations based on finite differences, was chosen for this application.

Equations (2.1), (2.2), (2.3), and (2.6) were discretized into crystallizer length steps (Δx), and crystal size steps (ΔL). Computation of the solution began with the population balance. The population density was then used in the solute mass balance to provide a new solute concentration. The explicit recursion expression for the population balance equation is:

$$n(i+1,j) = n(i,j) + \left(\frac{-G}{u_x}\right)\left[\frac{n(i,J+1) - n(i,j-1)}{2\Delta L}\right]\Delta x + \left\{\left(\frac{G}{u_x}\right)^2\left[\frac{n(i,J+1) - 2n(i,j) + n(i,j-1)}{(\Delta L)^2}\right]\right\}\frac{(\Delta x)^2}{2} \tag{2.7}$$

Population density from equation (2.7) can be converted to mass based distribution using the relationship:

$$w(L) = \rho k_v n_{calc} L^3 \Delta L \tag{2.8}$$

where n_{calc} is the population density calculated with population balance equation (2.7) and $w(L)$ is the mass based CSD (%).

To obtain a first approximation to the population balance equation (2.3), the mass balance equation (2.6), the nucleation (2.1) and crystal growth kinetic expressions (2.2), initial values for the vector of model parameters $\theta = [k_g, g, k_b, b]$ were assumed. The value of the parameters θ was

recalculated by solving an optimization problem until a minimum value for the objective function $\Phi(\theta)$, defined as the sum of squares of the error, was found. The error was defined as the difference between the obtained experimental measurement (y_{exp}) and the model prediction for crystal size distribution (y). The optimization problem is expressed as:

$$\min_{\theta} \Phi(\theta) = \sum_{0}^{L_{max}} \left[(y_{exp} - y(L))^2 \right] \tag{2.9}$$

subject to equations (2.1), (2.2), (2.3), and (2.6)

2.4 Crystallizer Selection and Design

2.4.1 Residence Time Distribution

Fluid elements may require differing lengths of time to travel though the reactor. The distribution of the exit times, defined as the *E(t)* curve, is defined as:

$$\int_{0}^{\infty} E(t)dt = 1 \tag{2.10}$$

The average residence time is given by the first moment of the age distribution:

$$t_m = \frac{\int_0^\infty tE(t)dt}{\int_0^\infty E(t)dt} = \int_{0}^{\infty} tE(t)dt \tag{2.11}$$

If there are no dead or motionless zones within the reactor, then t_m will be equal to τ, the residence time calculated from the total reactor volume and the volumetric flow rate of the fluid $\tau = V/v$.

The residence time distribution (RTD) of a reactor can be used to compare its behavior to an ideal reactor model. One model is the ideal plug flow reactor (PFR) in which the fluid is perfectly mixed in the radial direction but not in the axial direction. The RTD behavior of an ideal plug flow reactor is the narrowest RTD that can be maintained by using a continuous mode operation. Another model is the ideal continuous stirred-tank reactor (CSTR), in which the inlet flow is completely and instantly mixed into the bulk reactor. At all times, the reactor and the outlet flow have homogeneous compositions (Fogler, 2006).

2.4.2 Investigation of a suitable reactor concept

Crystallization reactors should be built with decisive single-use components for applications in pharma and fine chemicals to reduce cleaning effort and quality control. An easy scale-up, a wide operation window regarding flow rates, low investment costs, and a compact design should be taken into consideration when choosing an appropriate reactor. To achieve the desired reaction rates, yield, selectivity and product quality, a narrow residence time distribution is essential (Klutz, et al., 2015).

A continuous reactor built with a straight tube is characterized by a parabolic velocity profile, in which the elements nearby the wall have low velocities and thus very long residence times in comparison to the fast flowing fluid elements in the center of the tube. A broad RTD discards the straight tube as a suitable reactor, however, by decreasing the inner tube diameter and/or increasing the volume flow rate, it is possible to reach turbulent flow regime (Re > 2300). Turbulent flow has the advantage of maintaining strong radial mixing within the tube, thus an ideal plug flow reactor behavior is achieved (Klutz, et al., 2015).

In the case of long residence times caused by high flow velocities, strong disadvantages of this design are the long tube and high pressure losses. At laminar flow conditions, an alternative that obtains a narrow RTD with a smaller reactor size is to improve the mixing within the reactor. Similar types of mixing can result in identical RTD behavior in different reactors (Klutz, et al., 2015).

2.5 Mixing

At laminar flow conditions, mixing relies solely on molecular interdiffusion (Hessel, et al., 2005). Fick's first law of diffusion defines the time course of the transfer of a solute between two compartments that are separated by a thin membrane, given by:

$$\frac{dq}{dt} = -DA\frac{dC}{dx} \tag{2.12}$$

where q is the quantity of solute, A is the membrane surface area, C is the concentration, D the diffusion coefficient, dx the membrane thickness and dC/dx the concentration gradient. According to Fick’s first law, in the case of a solution made up of a solute in a solvent at two

different concentrations, the solute molecules would diffuse from the region of high concentration to the region of lower concentration, and the solvent molecules would diffuse in the opposite direction.

In this system, mass transfer takes place at the interface of the two liquids. Increasing the contact area between the reactants decreases the mass transfer limitation in the system leading to a decrease in the overall reaction time (López, Process Intensification Technologies for Mass-Transfer Limited Reactions: Case of Study Biodiesel Production. PhD Thesis., 2017). Consequently, and as can be observed from equation (2.12), the efficient maximization of the interfacial surface area and concentration gradient is the guiding principle of micromixers (Hessel, et al., 2005).

In a crystallization process, insufficient agitation causes a crystal growth rate controlled by the rate of solute transfer from the bulk solution to the crystal-liquid interface. This is an undesirable process because the crystal growth rate obtained is usually significantly slower than the rate that would be obtained if interfacial attachment kinetics were the rate-controlling step (Myerson, 2002).

With this in mind, a crystallization mixer must fulfill two main requirements. First, it must bring the components of the mixture into close intense contact in order to reach a high degree on homogeneity between the solution and the antisolvent. Second, being that crystallization is a two-phase process, mixing needs to dissipate enough energy to keep the particles in suspension. Maintaining a high mass transfer rate to minimize supersaturation gradients in the film around a growing crystal is one of the primary functions of mixing in a crystallization operation (Alvarez, 2009).

In antisolvent crystallization good mixing conditions are essential to avoid creating local regions of high supersaturation whilst other regions are undersaturated (Myerson, 2002). Uneven saturation conditions can considerably affect the properties of the product including particle size distribution, morphology and purity. If the solution is not completely mixed before the crystallization starts, the crystallization proceeds under conditions of partial segregation (Alvarez, 2009).

A homogeneous state in a mixing process is accomplished by enhancing secondary-flow patterns superposed to the main flow or by redistributing and recombining the components of the mixture (Hessel, et al., 2005; Alvarez, 2009).
Mixing mechanisms can be broadly classified as active or static.

2.5.1 Active Mixing

In active mixing, an external force supports the system and thus mixing is enhanced. Several methods can be utilized like ultrasonic micromixers, pulse flow mixers, thermal bubble mixers, and acoustic mixers (Klutz, et al., 2015).

2.5.1.1 Novel Active Mixing Crystallizers

Recent antisolvent crystallization of APIs in continuous crystallizers using active mixing include the work by Lee et al. (2016), who compared the crystallization of L-threonine in a Couette-Taylor (CT) crystallizer to a mixed-suspension mixed product removal (MSMPR) crystallizer. Continuous Couette-Taylor crystallizers consist of two concentric cylinders, of which the inner cylinder rotates freely. When the rotation speed of the inner cylinder exceeds a certain value, a unique Couette-Taylor vortex is formed, which has a significant effect on the crystallization process (Nguyen A. K., 2010). A MSMPR crystallizer is one of the most common continuous crystallizers at present. Products with narrow crystal size distribution (CSD), and high yield and purity, can be obtained by using MSMPR crystallizers (Farmer, 2016). Distilled water was used as the solvent and methanol as antisolvent. It was proven that mean crystal size was reduced when increasing the rotation/agitation speed. In the CT crystallizer mean crystal size decreased from 50 μm to 36 μm, while in the MSMPR crystal size decreased from 90 μm to 70 μm. The crystal size produced in the MSMPR crystallizer was almost two times larger than those produced in the CT crystallizer; this is due to the promotion of nucleation by the periodic fluid motion in the CT crystallizer. A crystal recovery in the CT crystallizer was always 2-3 fold higher than that in the MSMPR crystallizer.

Nguyen et al. (2012), who evaluated the crystallization of guanosine 5-monophosphate (GMP) using distilled water as solvent and methanol as the antisolvent, studied a multiple feed mode CT crystallizer. The effect of the number of antisolvent and solution points on mean crystal size, crystal recovery, and time phase transformation was studied. It was observed that when operating

the CT crystallizer with three antisolvent and three solution addition points, the phase transformation was at least 2 times faster than the phase transformation with the conventional mode, and 10 times faster when compared to the phase transformation in a continuous MSMPR crystallizer. In this configuration, a GMP mean crystal size of 52 µm was obtained, compared to a 50 µm in the conventional mode. For all feeding modes, the crystal size became larger along the axial position of the crystallizer. This is due to the continuous growth of the crystals formed in the entrance of the crystallizer, which became seeds for the phase transformation in along the reactor.

A relatively new type of continuous crystallizer is the continuous oscillatory baffled crystallizer (COBC) that consists of a series of tubes with some baffles periodically arranged inside. The movement of bellows produces a repeating cycle of vortices, which can create strong radial motions (Wang, et al., 2017). The antisolvent crystallization of salicylic acid (an API substitute) in a COBC was studied by Brown et al. (2015). It was concluded that that mean crystal size increased with an increase in mixing intensity; the effect of supersaturation on experimental steady states was also studied, however, mean crystal size behavior responded in a more complex way due to the occurrence of desupersaturation. The operating conditions for an extended operation of 6.25 h were determined and an average crystal size of 44.63 µm was obtained.

2.5.1.2 Tubular Active Mixing Crystallizers

Tubular crystallization reactors can eliminate problems such as inhomogeneous mixing and the need for rapid stirring. The high surface to volume (compared to stirred-tank crystallizers) facilitates rapid heat exchange and provides accurate control of the temperature processed medium and the supersaturation profile (Besenhard, et al., 2015).

Recent crystallization of APIs in continuous tubular crystallizers include the work by Besenhard et al. (2015) who studied the control of the mean crystal size within a broad range on the basis of a seeded cooling crystallization process of acetylsalicylic acid from an ethanol solution. An ultrasound seed generation method was used to produce sufficiently small seed crystals and a generic response function L_{mean} (V_{seed}) was defined. To examine the feedback controller, the mean crystal size was tuned to five target values: 130 µm, 120 µm, 110 µm, 100 µm, and 90 µm.

All target sizes were reached in less than three control steps, thus demonstrating the potential for highly accurate crystal size tuning in a tubular crystallizer.

Furuta et al. (2016) studied the continuous crystallization process of an API using a sonicated tubular system. For comparison purposes, a simple addition batch system and a premixing semi-batch system were also studied. In both of these systems, agitation speed and addition rate were varied in order to find the best operation conditions for obtaining a desired crystal size within a 1-7 μm range. In the simple mixing batch system this was impossible to achieve, while in the pre-mixing system it was possible to control the mean crystal size in the range of 10-30 μm. The sonicated tubular crystallizer gave the desired particle size and no blockage was reported. It was concluded that since productivity is still lower than that of the current batch process, further investigation will be necessary to replace the batch crystallization with continuous crystallization using a wider and/or longer tube, while keeping the residence time constant.

Tubular devices disadvantages include difficult slurry handling, as they are prone to settling of solids, wall scaling, and clogging. Coiled tubes are usually operated without intense pulsation, except a moderate forward pulsation of the peristaltic feed pumps, which are usually applied. Thus, the slurry transfer is solely achieved by the net fluid flow. Additionally, these devices are operated in the laminar flow regime, which has a limited mass transfer that results in a wide RTD (Hohmann, et al., 2018).

On the other hand, active mixers are complicated to operate, expensive to fabricate and prone to failures more than passive mixers (Klutz, et al., 2015).

These issues motivate further research in obtaining simple and effective crystallizers without compromising product quality.

2.5.2 Passive Mixing

Static or passive mixers are devices that promote mixing of fluids in a pipeline without moving parts (Alvarez and Myerson, 2010). Passive mixing can be classified in two broad mechanisms (Klutz, et al., 2015). The first enhances mixing by contacting the inlet streams of the mixer, or injects substreams into the main stream. Some of the proposed devices that ensure good mixing in antisolvent crystallization processes are confined impinging jets and tee-mixers.

Recent crystallization of APIs in continuous crystallizers using passive mixing includes the work by Liu et al., (2016). In this paper, an already proposed process design (Liu, 2015) that has an impinging jet mixer submerged in the solution of a batch stirred tank crystallizer was modified to operate in a continuous mode. The impinging jets mixed the fluids intensively prior to reaction and nucleation, dispersing the small particles to minimize their aggregation and thus promoting crystal growth. Afterwards, the solution flows into a tubular reactor for crystal growth. In the reactive crystallization of sodium cefuroxime (an antibiotic), it was found that the new design produced crystals of higher crystallinity, narrower particle size, and improved product stability, than batch crystallizers.

Additionally, Jacqueline et al., (2016) studied the crystallization of the hydrophobic drug LASSBio-294. Two pre-mixers (Roughton and T-mixer) were tested in stirred vessel in order to investigate the mixing effect on the crystal properties. A reference experiment without pre-mixer was conducted for comparison. It was found that the mean volume size obtained without pre-mixer is higher than those obtained with pre-mixer.

Unfortunately, since it is difficult to align and maintain the alignment of the impinging jet fluid streams, and various parts of the impinging jet apparatus tend to clog easily, the scale-up of these devices for large-scale production is complicated (Alvarez and Myerson, 2010).

The prototypical design of the second passive mixing mechanism is a series of identical, motionless inserts called elements that redistribute fluid in the directions transverse to the main flow. Geometries like ridges, bends or herringbones perturb the flow along the mixer, where the inlet solutions have been introduced into the same channel. The performance of this redistribution is a function of the specific design and number of elements (Klutz, et al., 2015), (Thakur, et al., 2003).

Motionless mixers typically have lower energy consumptions and reduced maintenance requirements because they have no moving parts. They offer a more controlled and scalable ratio of dilution in fed batch systems and provide homogenization of feed streams with a minimum residence time (Thakur, et al., 2003). The advantages of static mixers over conventionally agitated vessels are given in **Table 2.1**.

Table 2.1. Potential Advantages of Static Mixers Compared to Mechanically Agitated Vessels (Thakur, et al., 2003)

Static mixer	Continuous stirred-tank reactor (CSTR)
Small space requirement	Large space requirement
Low equipment cost	High equipment cost
No power required except pumping	High power consumption
No moving parts except pump	Agitator drive and seals
Small flanges to seal	Small flanges plus one large flange to seal
Short residence times	Long residence times
Approaches plug flow	Exponential distribution of residence times
Good mixing at low shear rates	Locally high shear rates can damage sensitive materials
Fast product grade changes	Product grade changes may generate waste
Self-cleaning, interchangeable mixers or disposable mixers	Large vessels to be cleaned

The scale-up of mixing processes in a pipeline with static mixers is less complicated than other process configurations because of its relatively simple hydrodynamics. Although static mixers have been successfully used in the plastic, polymer, and oil industry, the literature to their manufacture of pharmaceutical compounds is limited to the use of static mixers only at the entrance of the reactor (Alvarez and Myerson, 2010).

2.6 Coiled Flow Inverter (CFI)

On the cross-sectional plane of a straight helix tube, Dean symmetrical vortices are formed due to the presence of secondary flow, generated by the action of unbalanced centrifugal forces (W. R. Dean, 1928). The intensity of the secondary flow in radial direction is measured by the Dean number, which is defined as the ratio between centrifugal and viscous forces:

$$De = Re \cdot \sqrt{\frac{d_i}{d_c}} = Re \cdot \sqrt{\frac{1}{\lambda}} \qquad (2.13)$$

where d_i is the inner tube diameter, d_c is the coil diameter, and λ is defined as the curvature ratio of the helical tube. As Dean number increases, chaotic advection surpasses molecular diffusion as the main mechanism of transport thus enhancing heat and mass transfer under laminar flow conditions (Mridha and Nigam, 2007).

These secondary vortices stabilize the flow of a liquid in a helical coil mixer, improving radial mixing and preventing turbulence. The result is near plug flow characteristic which is very well mixed compared to a straight tube while retaining a small pressure drop (Bassett and de Graaff). The formation of centrifugal instabilities in the feed flow creates higher vorticity and shear rates at the wall of the coil thus provides stronger mixing effect than Taylor vortices (Vashisth and Nigam, 2009).

Mridha and Nigam (2007) studied the Dean vortices generated in a straight helical tube and found that the fluid present near the core of the confined regions of the vortices does not mix properly and remains trapped (**Figure 2.2a**).

Mixing can be further enhanced by producing some chaos in the fluid. Saxena and Nigam (1984) introduced a novel device of flow inversion achieved by bending the helical coil. Multiple flow inversions were achieved at low flow rates by changing the direction of centrifugal force inside the helically coiled tubes. After studying the effect of different design parameters on mixing, the best configuration consists of finite number of 90-degree bends (Mridha and Nigam, 2007). This design is presented in **Figure 2.1.**

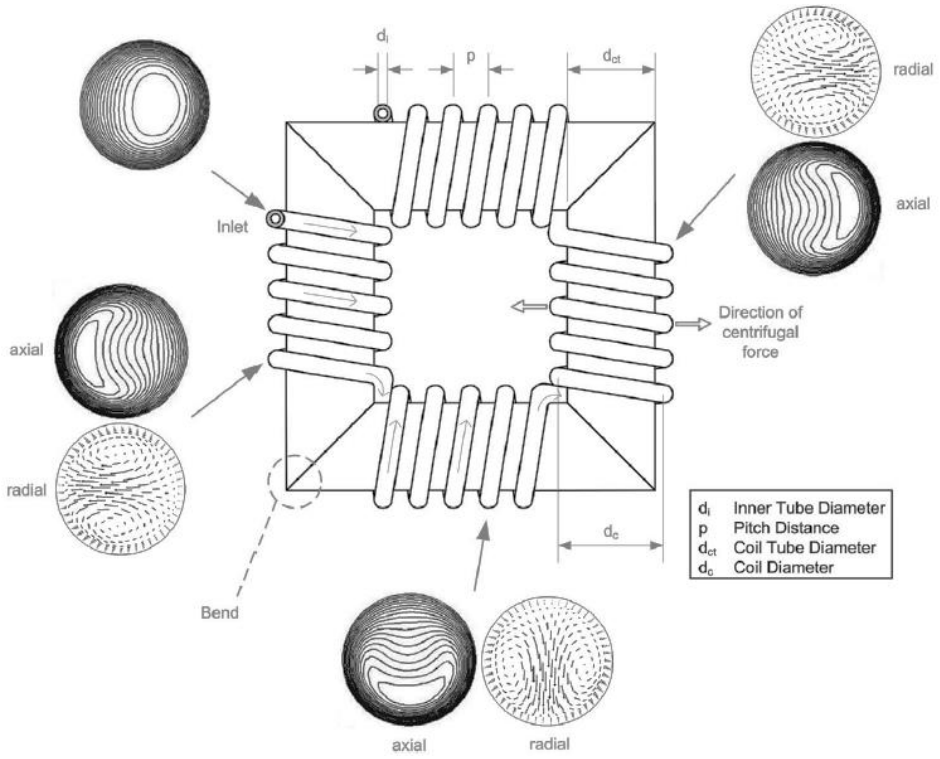

Figure 2.2. Geometry of the CFI system with corresponding axial velocity profiles showing the effect of centrifugal force (Klutzet al., 2015).

Figure 2.2 displays the computed Dean vortices for Re=15 at the outlet of a straight helical coil and CFI with one, two, and three 90-degree bends. After every equally spaced 90-degree bend, the Dean vortices were rotated 90-degrees due to the rotation of the plane of vortex. The increase in radial mixing of the fluid caused a gradual spread of the concentration profiles and an increase in the uniformity of concentration contours after each bend. The inversions of the flow consequently improve the mixing efficiency in the CFI with an increase in the number of bends, thus proving to be an efficient in-line mixer (Mridha and Nigam, 2007).

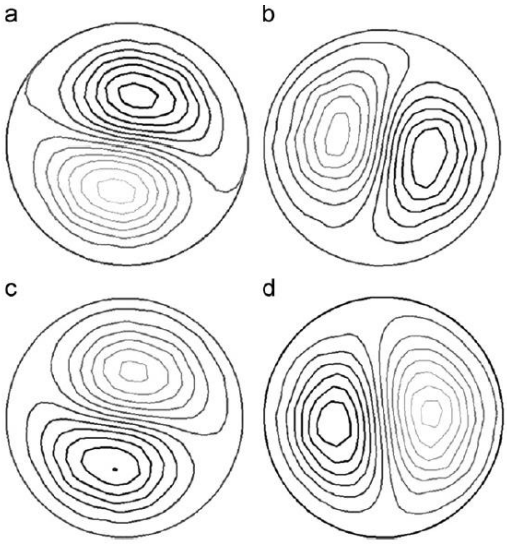

Figure 2.3. Fully developed Dean vortices for fluid with Re= 15 at outlet of (a) straight helical coil, (b) CFI with one bend, (c) CFI with two bends, (d) CFI with three bends (Mirdha and Nigam, 2007)

2.6.1 CFI geometry configuration

Helical tube reactors, and more specifically CFI reactors, have a significant advantage over both active and passive reactors in enhancing mixing and obtaining a narrow RTD. Literature (Klutz, et al., 2015; Vashisth and Nigam, 2009) has suggested the following parameters as characteristic of the CFI geometrical design, which are shown in **Figure 2.2:**

- *Inner tube diameter (d_i)*: Inner tube diameter is directly linked to Reynolds number. When volume flow rates and required residence time are kept constant, decreasing tube diameter leads to an increase in tube length due to higher flow velocities.
  Additionally, in the case of a CFI crystallizer, significantly lower crystal sizes compared to d_i can lead to settling of particles, which can further lead to unsteady operation, or even clogging of the device (Hohmann, et al., 2016). In order to avoid this phenomenon, and to have a compact CFI system, large inner tube diameters are desirable.
- *Coil radius (r_c)*: The coil radius r_c, with $r_c=0.5\times d_c$, where d_c is the coil diameter, influences the presence of secondary flow patterns within the CFI. If $r_c >> d_i$, secondary flow patterns will not appear. Additionally, r_c affects the compactness of the CFI by allowing a higher number of turns to be incorporated if a small coil radius is used.

- *Tube wall thickness*: An increased tube wall thickness leads to an increase in the length of the straight helix elements for a given number of turns, affecting CFI compactness. A small wall thickness is thus preferable.
- *Pitch distance (p)*: An increased pitch distance leads to an increase in the length of the straight helix element for a given number of turns, affecting CFI compactness. Consequently, pitch distance should be kept at its minimum value, when there is no space between each turn, which translates to $p=d_0$, where d_0 represents outer tube diameter.
- *Dean number (De)*: The Dean number is a dimensionless number that characterizes the strength of secondary flow patterns. It can be calculated according to equation (2.13). Saxena and Nigam (1984) reported that an increased Dean number results in a gradual narrowing of the RTD. It was reported that a secondary flow is fully developed for $De>1.5$ and that *De* should have a minimum value of 3 in order to obtain a narrow RTD.
- *Dimensionless Pitch (H):* A smaller value of *H* denotes velocity contours symmetrical to the centerline of the tube. As the coil pitch is increased, the velocity contours become asymmetrical. *H* can be calculated by the following expression:

$$H = \frac{p}{2 \cdot \pi \cdot r_c} \tag{2.14}$$

- *Torsion parameter (T):* In the case of helically coiled structures Torsion parameter *T* is defined as:

$$T = \frac{p}{2 \cdot \pi \cdot r_c \cdot Re} \tag{2.15}$$

  The Torsion parameter is a dimensionless number that combines the geometrical ratio of pitch distance and the length of one turn within a helical coil with the Reynolds number.

  T describes how strong the coiled reactor's geometry differs from a straight tube reactor, as an unlimited pitch distance finally leads to a straight tube reactor.

  Saxena and Nigam (1983) investigated the effect of Torsion parameter on RTD and concluded that the narrowest RTD was obtained for $T \approx 0$. In the range of $0<T<0.001$, the effect of Torsion parameter is not significant; however, in the range of $0.001<T<0.005$ a broad RTD curve is obtained. Therefore, for a narrow RTD, it would be better to have *T* less than 0.001.
- *Number of turns in one coil:* At least two turns are required in order to have fully developed secondary flow in the cross-sectional plane (Saxena and Nigam, 1984).

- *Number of 90-degree bends*: Increasing the number of bends drastically narrows RTD of the CFI. The narrowest RTD is obtained for equal lengths of coil before and after the 90-degree bend. A parameter that characterizes the performance of a CFI is defined as*:*

$$R_A = \frac{1}{1 + n_{bends}} \tag{2.16}$$

The lower the value of R_A, the narrower is the RTD (Saxena and Nigam, 1984).

Klutz et al., (2015) varied these parameters in order to obtain the "best performance" CFI design. It was found that the number of 90-degree bends was the most significant factor in obtaining a narrow RTD, which is in accordance with the results given in literature (Saxena and Nigam, 1984).

2.6.2 CFI Crystallization

Wiedmeyer et al. (2017) studied the cooling crystallization of potash alum dodecahydrate in helically coiled flow tube (HCT) using deionized water as solvent and previously seeded crystals of different sizes. The purpose of the investigation was to study the HCT as a basic subunit of the CFI. The main finding of this work is that there is a size-dependent particles residence time in the laminar flow region. For a flow of 0.24 m/s, large crystals (167 μm) were faster and had a shorter residence time (430 s) than smaller crystals (81 μm and 670 s of residence time). For a flow of 0.35 m/s, the effect of size dependent separation was not observed.

In order to explain this behavior, numerical simulations were performed for a representative part of the HCT, which showed the formation of a secondary flow with two vortices. It was hypothesized that since the secondary flow has less strength than the main flow, only small crystals can be transported along such vortices, while larger crystals follow the main flow direction through the tube. This allows small crystals more time to grow, narrowing the CSD and therefore making the HCT design advantageous in comparison to other continuous crystallizers.

Besenhard et al. (2017) also studied size-dependent particles residence time in a HCT. Three sieved fractions of D-mannitol were suspended in a saturated solution of 60% ethanol and 40% water. The size fractions were large (150−180 μm), medium (90−150 μm), and small (50−80 μm) and three different flow rates were used: low (8.7 ml/min), moderate (13.7 ml/min), and high (18.7 ml/min). Recorded images of the suspension showed that at a slow flow rate, crystals

of the three sizes accumulated at the rear end of the slug. At a moderate flow rate, only the smaller crystals were dispersed homogeneously; while at a high flow rate, large crystals were dispersed but not homogeneously. This shows that as a particle grows in size, the larger the fluid strength needed to influence the particle's movement.

Hohmann et al. (2016) developed a continuous cooling tubular crystallizer, based on the coiled flow inverter design. A compact design with five turns per segment, nine segments and eight 90-degree bends was constructed. L-alanine was crystallized with deionized water as solvent. In the first and second experiments, mass flow rates of 8.80 g/min and 4.95 g/min were used. In both experiments a homogenous solution, in which no particles were detected, was obtained in the outlet. In the third experiment, the mass flow rate of the solution was further reduced (2.34 g/min) to increase the mean residence time. Approximately, two mean residence times after start-up, small crystals with an estimated mean size of 40 μm and narrow size distribution were obtained in the product stream. After 2 h, large agglomerates could no longer be fluidized at the low flow velocity which led to tube clogging. It was concluded that in a continuously operated tubular crystallizer, operation characteristics such as mean residence time, RTD, and particle fluidization directly depend on the mean flow of the solution/suspension, resulting in a reduced degree of freedom for choosing operating conditions compared to conventional batch systems.

Hohmann et al. (2018) carried further investigation in the previously described crystallizer design. The seeded cooling crystallization of L-alanine from an aqueous solution was investigated both in a stirred batch vessel crystallizer and in the continuous horizontal CFI crystallizer. In the batch processes, the obtained median crystal size (112.3 μm) was larger compared to the product crystals from the continuous process (107.83 μm). This was attributed to the limited mean residence time under the investigated conditions in the CFI crystallizer setup. For a flow rate of 40 g/min in the CFI system, less sedimented crystals were observed and a more homogeneous crystal distribution in the tube cross section was obtained. For this homogeneous suspension flow conditions, it was determined that the CFI crystallizer is promising equipment for transferring crystallization processes from batch to continuous mode while maintaining the product quality with a narrow CSD.

3. Experimental section

3.1 Materials

Flufenamic acid is a potent nosteroidal drug with analgesic, anti-inflammatory and antipyretic properties. It is marked to treat rheumatoid arthritis and osteoarthritis. This drug is a weak acid soluble in organic solvents as methanol, ethanol, chloroform, and acetone, and it has very low solubility in water. It has been reported that flufenamic acid has up to seven different crystal forms, although forms III and I are the most commonly encountered (Alvarez and Myerson, 2010). Its chemical and physical properties are presented in **Table 3.1**. Flufenamic acid was purchased from Fisher Scientific. Ethanol (99.9%) was used as the solvent and distilled water as the antisolvent.

Table 3.1 Flufenamic Acid Physical and Chemical Properties **(Drug Bank, 2018)**

Parameter	Value
Chemical formula	$C_{14}H_{10}F_3NO_2$
Average Weight [kg/kmol]	281.2299
Density[kg/m^3]	1501
Shape factor (k_v)	$\pi/6$

3.2 Apparatus

All the reactor systems were manufactured by coiling stainless-steel tubing with an internal diameter (d_i) of 3 mm on a supporting structure. A coil diameter (d_c) of 30 mm was kept in order to achieve a curvature ratio (λ) of 10. The curvature ratio and the number of turns for each 90-degree bend were selected based on values reported in literature (López-Guajardo, et al., 2017; Mridha and Nigam, 2007).

The active pharmaceutical ingredient (API) solution and antisolvent were fed into the system through a 1/4” OD T connector that conducts both flows directly inside the static mixer using 1/8" tygon tubing. Flow of solution and antisolvent were controlled with peristaltic pumps (Control Company Mini-Pump Variable Flow Reversible Flow Peristaltic Pump 3384CC). Antisolvent solution was contained in a 200 mL beaker, and API solution in a 100 mL flask.

Literature suggests there is no major significant difference in the residence time of particles for upward and downward flow in a vertical helically coiled tube (Wiedmeyer, et al., 2017), and that the orientation of helical coils has no significant impact on the crystallization process and product quality (Hohmann, et al., 2018). With this in mind, a specific CFI orientation was not procured. The CFI was clamped in a retort stand ensuring that the fluids entered the device at a straight angle, as well as certifying that the system orientation remained constant.

At the CFI outlet, a sample (approximately 20 mL) of the flowing slurry was quickly filtered with a 21 mm microfiber filter (Whatman Glass Microfiber) under a vacuum (GE Commercial Motors Vacuum Pump 1/4 HP 1725 RPM) to determine solute concentration by gravimetric analysis. Crystal size distribution of the solid product was characterized by image analysis of at least twelve crystal pictures obtained from optical microscope (Omax Professional Plan Laboratory Trinocular Compound Microscope) used with a 20x magnification.

3.2.1 Multiple Antisolvent Injection Points Crystallization Experiments

A CFI system consisting of 16 equally spaced turns was fabricated in order to evaluate the effect of the number of antisolvent injection points. Three 90-degree bends were introduced after every four turns; hence, each helical tube segment has the same length before and after the bend. The CFI had a calculated volume of 18 mL and its design parameters are summarized in **Table 3.2.**

Table 3.2. CFI Design Parameters for Multistage Antisolvent Addition

Parameter	Value
d_i [mm]	3
d_o [mm]	6
p [mm]	6
d_{ct} [mm]	24
d_c [mm]	30
n_{turns} [-]	16
n_{seg} [-]	4
n_{bends} [-]	3
l [m]	2.10

In experiments with one injection point, 100 % of the antisolvent is injected at point 1. In experiments with two injection points, 50% of the antisolvent is injected at point 1 and 50% at point 2. In the case of three injection points, one third of the antisolvent is injected at points 1, 2, and 3. A schematic process flow diagram of the multiple CFI system antisolvent injection points is presented in **Figure 3.1a**. A picture of the CFI adapted configuration that allows the antisolvent injection in different points can be seen in **Figure 3.1b**.

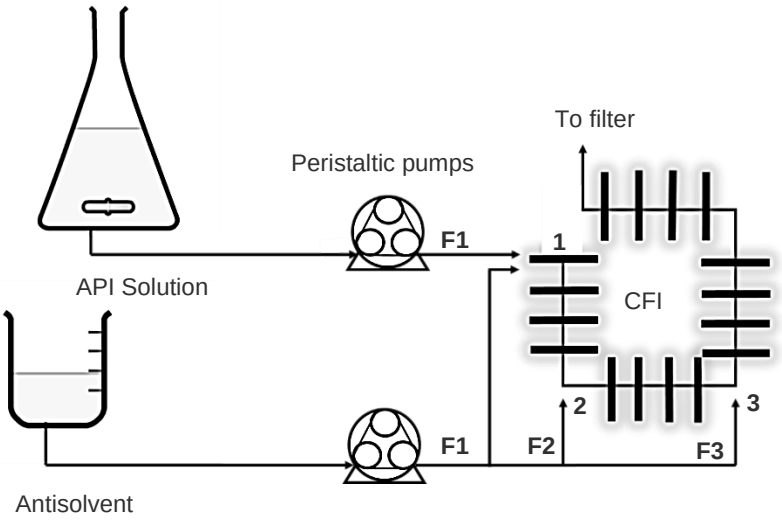

(a)

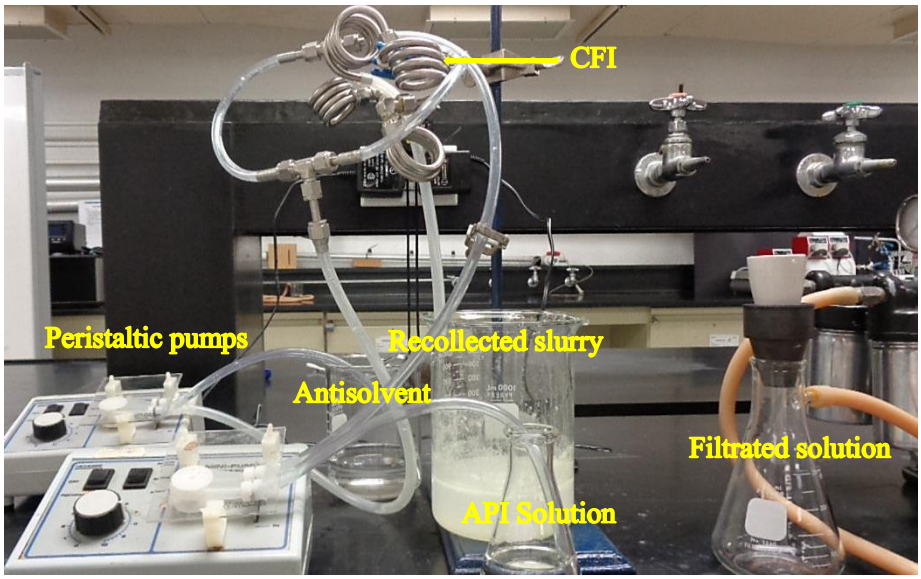

(b)

Figure 3.1. (a) Schematic Process Flow Diagram of the Continuous Crystallization System with Multistage Antisolvent Addition (b) Picture of Adapted CFI

3.2.2 CFI Configuration (varied number of 90-degree bends) Crystallization Experiments

The effect of the number of 90-degree bends on the crystallization process was evaluated. This required the construction of four crystallization reactors, in which the total number of turns was kept at a constant value of twelve. The four constructed reactors had a calculated volume of 14 mL each, and its resulting design parameters are summarized in **Table 3.3.**

Table 3.3. CFI Design Parameters for Varied Number of 90° Bends

Parameter	**Value**			
d_i [mm]	3			
d_o [mm]	6			
p [mm]	6			
d_{ct} [mm]	24			
d_c [mm]	30			
n_{turns} [-]	12			
n_{seg} [-]	1	2	3	4
n_{bends} [-]	0	1	2	3
l [m]	1.5			

The first reactor was a straight helical tube with twelve turns (**Figure 3.3a**). The second reactor was a CFI crystallizer with two segments of six turns each, connected by one 90-degree bend (**Figure 3.3b**). The third reactor was a CFI with three segments of four turns each, connected by two 90-degree bends (**Figure 3.3c**). The third reactor was a CFI with four segments of three turns each, connected by three 90-degree bends (**Figure 3.3d**).

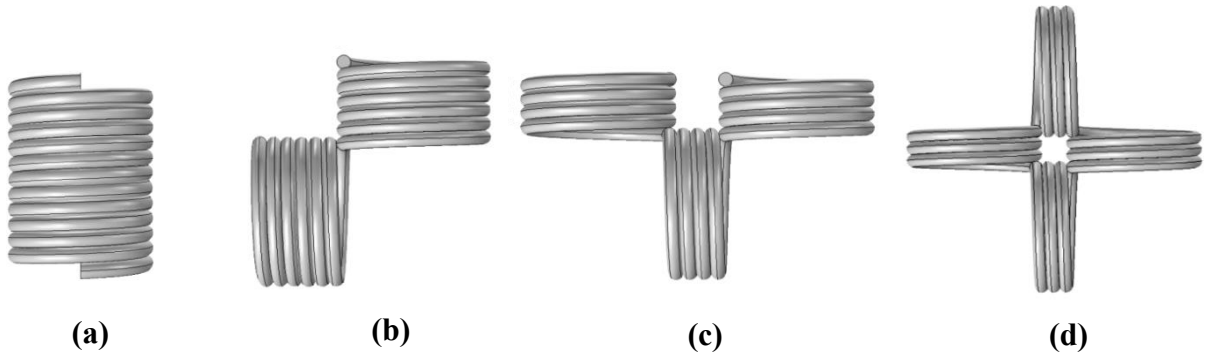

Figure 3.2 Geometries of the reactors used (a) Helical Reactor; (b) One 90-degree bend; (c) Two 90-degree bends; (d) Three 90-degree bends

3.3 Procedure

All experiments were conducted at constant room temperature (25°C). The effect of the number of injection points of antisolvent on crystal size distribution was evaluated with flufenamic acid. A solution of flufenamic acid in ethanol (12.4 mg/mL) with a flow rate of 25 mL/min was mixed with water (antisolvent) in the CFI with a corresponding flow rate of 50 mL/min. The flow rate of antisolvent added to the reactor was chosen to maintain a ratio solution/antisolvent of 1:2 vol/vol in all experiments.

Experiments were conducted with 1, 2, and 3 points of addition of antisolvent, corresponding to one flow of 50 mL/min, two flows of 25 mL/min, and three flows of 16.67 mL/min, respectively. Additionally, the effect of the crystallizer geometry on crystal size distribution was studied by running experiments with four different crystallizer configurations: helical coil, one 90-degree bend, two 90-degree bends, and three 90-degree bends. The corresponding physical properties of the used materials are given in **Table 3.4.**

Table 3.4. Physical Properties of the Solution in the Crystallizer

Property	Value	Reference
ρ_{water} (23°C) [kg m^{-3}]	997.50	(McCabe, et al., 2007)
$\rho_{ethanol}$ (23°C) [kg m^{-3}]	783.00	(Cengel and Boles, 2015)
ρ_{sol} (23°C) [kg m^{-3}]	926.76	-
μ_{water} (23°C) [Pa s]	8.90 e-4	(McCabe, et al., 2007)
$\mu_{ethanol}$ (23°C) [Pa s]	11.34 e-4	(Dortmund Data Bank)
μ_{sol} (23°C) [Pa s]	9.48 e-4	-

The continuous crystallization process needs a period of time to reach a steady state. The total duration of the experiments corresponded to six residence times. Each experiment had two runs, after which ethanol and subsequently air were injected to clean the system and remove any impurities.

At the CFI outlet, a sample (approximately 20 mL) of the flowing slurry was quickly filtered with a 21 mm microfiber filter (Whatman Glass Microfiber) under a vacuum (GE Commercial Motors Vacuum Pump 1/4 HP 1725 RPM) to determine solute concentration by gravimetric analysis. Crystal size distribution of the solid product was characterized by image analyses of twelve crystal pictures obtained from optical microscope (Omax Professional Plan Laboratory Trinocular Compound Microscope) used with a 20x magnification.

4. Results and discussion

This chapter evaluates the fabricated reactors' performance according to literature's proposed parameters, observed system operation during the experimental work, and comparison of experimental versus calculated crystal size distributions. The final section of this chapter evaluates the intensification of the crystallization process in terms of mean crystal size, coefficient of variation (CV), crystallization and pre-expansion temperatures, as well as extraction pressure.

4.1 Assessment of Process Design in terms of CFI Parameters

Literature has proposed several parameters in order to evaluate and guarantee the proper operation of a CFI reactor. These parameters include the cut size diameter x_{cut}, and the following dimensionless numbers: Stokes number (*St*), Reynolds number (*Re*), Dean number (*De*), curvature ratio (λ), dimensionless pitch (*H*), and Torsion parameter (*T*), which will be evaluated in this section. Since the configuration of the CFI used in this work has been successfully applied to intensify biodiesel production in the past (López-Guajardo, et al., 2017) it is an important matter to determine if this CFI design also intensifies crystallization processes.

Even though crystal fluidization is crucial for suspension crystallization purposes, the fundamental behavior of solid-liquid flow in small-scale tubular devices is still poorly understood (Hohmann, et al., 2016). It has been reported that low flow rates cause the formed crystals not to disperse properly, which leads to settling of particles inside the reactor. Under these conditions, pumps are not able to remove the particles, which eventually leads to clogging (Alvarez, 2009).

Settling of particles in the gravitational field is a well-known phenomenon in macroscale heat exchangers when being operated at nearly stagnant conditions. A simplified Stokes flow model was proposed to estimate particle sizes which are not affected by gravitational settling and remain fluidized in a helically coiled tubular device with Dean vortices flow (Hohmann, et al., 2016):

$$x_{cut} = \sqrt{\frac{72}{\pi}\frac{\mu_{sol}}{(\rho_p - \rho_{sol})g_c}\frac{\dot{m}}{\rho_{sol}d_i^2}} \quad (4.1)$$

where x_{cut} denotes the cut-size diameter, μ_{sol} the dynamic viscosity of the solution, ρ_p the density of the particles, ρ_{sol} the density of the solution, $\dot{m}$ the mass flow rate, g_c the gravitational constant, and d_i the internal tube diameter. This model describes a vertical straight tube fluidized by a suspension in the opposite direction of the gravitational force. This reflects the upward flow in a horizontally directed tubular coil.

Larger particles than the calculated cut-size diameter x_{cut} will sediment in the flow, while smaller particles will remain in the suspension. The model takes the tube geometry, the operating conditions, and physical properties into account. It does not consider the effect of Dean vortices, however, there is evidence that Dean vortices can considerably enhance particle fluidization compared to devices without them. In spite of the model limitations, it represents a viable method to estimate the allowable particle size of a tubular crystallizer to avoid sedimentation and clogging from a fluid dynamics perspective (Hohmann, et al., 2016). For the performed experiments, a minimum value of 546 µm was estimated for cut-size diameter x_{cut}, which means no clogging by gravitational settling should be observed if crystal particle sizes are smaller than this value. For details of these calculations, the reader may refer to **Annex A**.

In micro-channels operating at laminar flow condition, literature has suggested that some combinations of particles and wall materials might be unfavorable as they can cause scaling. Scaling can be caused by strong particle-to-surface attraction, that is, adsorption, adhesion due to surface roughness or heterogeneous nucleation of crystals on the wall surface. One way to estimate if these phenomena will occur is to analyze particle deposition controlled by diffusion, which takes place when particles have a particle diameter (d_p) smaller than 30 nm (López, 2017). Since this size range is too small for the crystals of this study, deposition controlled by diffusion will not be considered.

Scaling can also be caused by the mechanical entrapment of particles due to inertial impaction caused by unsteady changes in tube diameter or flow constrictions (Hohmann, et al., 2016). One way to estimate if this phenomena will occur is to analyze particle deposition controlled by

convection (inertia), which occurs when particles with d_p > 200 nm are accumulated in the contractions of pipes, expansions, elbows, and turns due to the interaction they have with the walls of the system and the speed of the flow (López, 2017). Deposition controlled by convection does not occur when the Stokes number, as defined by the following equation, is smaller than 0.05:

$$St = \frac{\rho_p \cdot {d_p}^2 \cdot u}{18\mu_{sol} \cdot d_i} \tag{4.2}$$

where ρ_p is particle density, d_p is particle diameter, u is the average fluid velocity, μ_{sol} the dynamic viscosity of the solution, and d_i the internal tube diameter. For the performed experiments, a minimum value of d_p = 125 µm was estimated in order to obtain *St* < 0.05, which means no deposition controlled by convection should be observed if crystal particle size is smaller than this value. For details of these calculations, the reader may refer to **Annex A**.

The final crystal shape is influenced by the time a crystal remains in the tube. A high *Re* improves mixing, whereas a low *Re* decreases the tube length, which is required to reach a certain residence time and thus growth (Wiedmeyer, et al., 2017).
Previous studies have covered certain Reynolds numbers for CFI crystallizers, depending on which different particles behaviors were observed. In the work by Hohmann et al. (2016), the operational Reynolds numbers were 8.5, 18, and 32. It was found that at *Re* = 32 and at *Re* = 18, the residence time in the CFI was not enough to induce primary nucleation, whereas at *Re* = 8.5, small crystals were obtained in the product stream.

Further work in the same CFI crystallizer (Hohmann, et al., 2018) was performed at *Re* = 110 and at *Re* =145 (unlike the previous experiments, spontaneous nucleation was avoided by the application of seed crystals). It was observed that at *Re* = 110, crystals sedimented on the tube surfaces before reentering the bulk flow, although no stagnant crystal settling nor wall scaling were observed. This flow behavior was less distinct at *Re* = 145, which corresponds to an elevated mass flow rate. This more homogeneous crystal distribution in the tube cross section was attributed to the increasing drag/lift forces of the fluid on the particles and the intensified Dean vortices with increasing flow rate.

It can be concluded that very low Reynolds numbers may result in clogging of the CFI or inhomogeneous crystal dispersion in the bulk flow, which may lead to a broad CSD. However, large Reynolds numbers may not give the system enough time to induce primary nucleation. For these reasons, working with the correct Reynolds number was of essential importance in this work.

Reynolds numbers in the range between 290 and 520 were used in the experiments of multiple antisolvent addition points, while a number of 520 was used in all experiments with a varied number of 90-degree bends. For this range of *Re*, Dean numbers in the range of 90-160 were obtained. These Dean values are in accordance to literature (Saxena and Nigam, 1984) since in a CFI, a narrow residence time distribution for Dean number values > 3 has been observed due to the interchange of velocities among the fluid elements of different ages caused by the shift in the direction of centrifugal force.

A curvature ratio of $\lambda = 10$ was used in all systems. According to literature, as the curvature ratio increases, flow behavior approaches that of a straight tube ($\lambda \to \infty$). This minimizes the curvature effect as centrifugal forces become less predominant for higher curvature ratio coils. In the case of $\lambda = 10$, a strong centrifugal force has been reported in previous studies (Vashisth and Nigam, 2009).

Dimensionless pitch was calculated as stated by equation (2.14), with a resulting value of 0.064, which is in the range of the work of Vashisth and Nigam (2009) for symmetrical velocity contours in helically coiled tubes.

Torsion parameter *T* was estimated according to equation (2.15), with a resulting value of 0.000127. *T* describes how strong the coiled reactor's geometry differs from a straight tube reactor. In order to obtain a narrow RTD, literature suggest *T* should be lower than 0.001 (Klutz, et al., 2015).

In all experiments, a uniform suspension of flufenamic acid crystals in the ethanol-water slurry at the CFI outlet was obtained. It can be concluded that the stainless-steel CFI with $\lambda = 10$ and $H = 0.064$, operated at $Re = 290\text{-}520$, with $De = 90\text{-}160$, and $T = 0.000127$ was successful in creating

uniform mixing conditions were system clogging was not observed. Consequently, narrow CSDs could be expected, which will be evaluated in the next sections.

4.2 Effect of the Number of Injection Points on CSD in Antisolvent Crystallization Experiments

In the CFI crystallizer, the mean crystal size of flufenamic acid was 32.86, 44.66, and 57.38 μm for 1, 2, and 3 points of antisolvent addition, respectively. In comparison, the mean crystal size for the Kenics crystallizer was 67, 80, and 94 μm for 1, 2, and 3 points of antisolvent addition (Alvarez and Myerson, 2010).

When compared to the CFI, obtained crystals were in average 1.8 and 2.3 times larger for the Kenics crystallizer and the crystallizer without static mixers, respectively (**Figure 4.1**).
Agitation is well known to reduce the induction time for primary nucleation (Besenhard, et al., 2017). Different authors have studied the crystallization of the same compound under different mixing conditions. In the work by Lee, et al., (2016) the crystal size of L-threonine produced in the MSMPR crystallizer was almost two times larger than those produced in the Couette-Taylor (CT) crystallizer. This behavior was attributed to a higher supersaturation induced in the inlet region of the CT crystallizer, which resulted in a higher population and smaller crystal sizes. Additionally, an elliptical Couette-Taylor crystallizer was studied (ECT) which produced slightly smaller crystals than the traditional CT crystallizer. This was attributed to the higher viscous energy dissipation in the ECT crystallizer, which resulted in a higher crystal nucleation and smaller crystal sizes. In the work by Nguyen et al. (2016) the mean crystal size of L-Lysine in the CT crystallizer was 13% smaller than that in the conventional stirred tank crystallizer. This was attributed to the effectiveness of the mixing condition in the CT crystallizer that promoted secondary nucleation.

Fluid dynamic motion influences crystal nucleation, where increasing the fluid motion increases nucleation (Lee, et al., 2016). Taking this in consideration, it can be hypothesized that the Dean vortices flow in the CFI are much more effective for inducing nucleation than the split and recombine flow profile achieved in a Kenics mixer.

As can be observed in **Figure 4.1**, mean crystal size increases as the number of antisolvent injection points increase. In the case of one injection point, the initial high supersaturation causes

the formation of a high number of small particles. In the experiments with two and three antisolvent points, a decrease in the initial antisolvent flow rate causes the initial supersaturation to decrease. As a result, fewer particles are formed and supersaturation is then consumed by crystal growth, resulting in particles of a bigger size. Therefore, as the number of antisolvent injection points increases, crystal growth dominates the crystallization process.

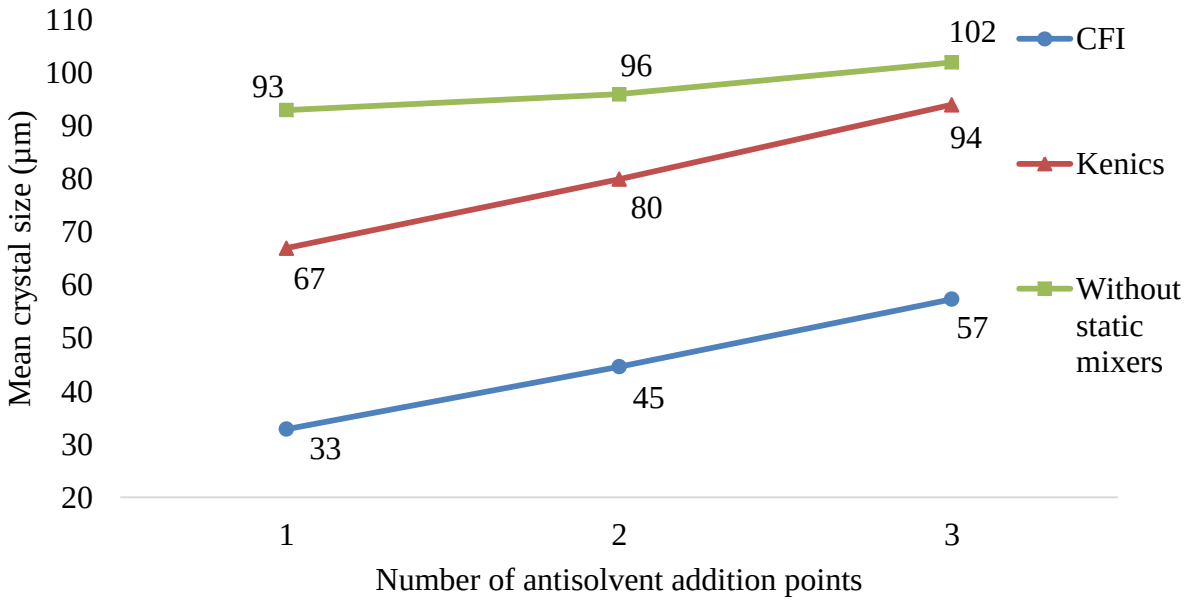

Figure 4.1. Effect of Three Different Mixers in Crystal Size Distribution of Flufenamic Acid (Kenics and Without static mixers data obtained from Alvarez, 2009)

In the experiments performed by Nguyen, et al., (2012), the effect of multiple antisolvent injection points was studied on the crystallization of guanosine 5-monophosphate (GMP) in a Couette-Taylor crystallizer. When the methanol antisolvent solution was injected only at the front end of the crystallizer, the mean crystal size obtained was 52 µm. When injecting the antisolvent solution in three equally distributed feed streams along the crystallizer, the mean crystal size slightly decreased to 48 µm. This was attributed to a longer regional mean residence time in the crystallizer in addition to a lower regional drowning-out ratio (a ratio of the antisolvent flow rate to the GMP feed flow rate in the region) inducing a lower regional supersaturation level that contributed to a facile phase transformation.

In the present study, even though the mean residence time of the crystallizer ($\tau = V/F_T$), defined as the total volume of the crystallizer (V) to total input flow rate to the crystallizer was the same (F_T), the regional mean residence time ($\tau = V_i/F_i$) defined as ratio of regional volume of

crystallizer (V_i) to input flow rate to the region (F_i) changed when increasing the number of antisolvent injection points. When using only one antisolvent injection point, the regional mean residence time at each region of the CFI would equally be $\tau/4$. However, when using multiple antisolvent injection points, the regional mean residence times in the crystallizer were varied as $\tau_1 = (V/4)/(F_1)$ in the first CFI segment, $\tau_2 = (V/4)/(F_{1+} F_2)$ in the second CFI segment, and $\tau_3 = (V/4)/(F_{1+} F_{2+} F_3)$ for the third and fourth CFI segments. This increase in the mean regional residence time, as well as the decreasing drowning-out ratio for the performed CFI experiments can be observed in **Table 4.1**.

Table 4.1. Regional Mean Residence Time and Drowning-out Ratio for CFI crystallizer

Number of Antisolvent Injection Points	**Solution Feed (mL/min)**	**Antisolvent Feed per Injection Point (mL/min)**			**Regional Mean Residence Time per CFI Segment (min)**				**Drowning -out Ratio**
		1	**2**	**3**	**1**	**2**	**3**	**4**	
1	25	50	0	0	0.06	0.06	0.06	0.06	2.00
2	25	25	25	0	0.09	0.06	0.06	0.06	1.00
3	25	16.7	16.7	16.7	0.11	0.08	0.06	0.06	0.67

While in the CT system presented by Nguyen et al., these variations in system conditions resulted in a smaller GMP crystal size, a bigger flufenamic acid mean crystal size was obtained in the CFI. This can be attributed to an induced supersaturation leading to a nucleation or crystal growth dominated process. This observation is consistent with the results reported by Alvarez and Myerson (2010) for the multiple antisolvent injection points crystallization of L-glutamic acid employing the Kenics crystallizer. Obtained mean crystal size first followed a decreasing pattern: 105 and 67 μm for 1 and 2 points of antisolvent addition, respectively. However, for 3 and 4 injection point, mean crystal size increased to 70 and 81 μm, respectively. These results, which can be consulted in **Annex B**, suggest that there is a breakpoint at which the system changes from being a nucleation dominated process to a crystal growth dominated process. In the case of the studied process for flufenamic acid in the CFI, the experimental results suggests it was growth dominated.

When comparing the coefficient of variation (CV) of crystal distribution with the Kenics crystallizer and a crystallizer without static mixers, smaller values were observed for the CFI, which indicate a higher mixing quality (**Figure 4.2**). A more detailed explanation of the reduced CV of CFI crystals will be addressed in section 4.4.

The experimental crystal size distribution of flufenamic acid for different antisolvent injection points is presented in **Figure 4.3**.The presented graphs were obtained from image analysis of a set of twelve pictures taken from each experimental run using an optical microscope (Omax Professional Plan Laboratory Trinocular Compound Microscope) used with a 20x magnification. Graphs in **Figure 4.3** present a similar width and a tendency of the graphs moving towards a larger mean crystal size as the number of addition points increases can be observed. In **Figure 4.3,** the presented pictures were selected as representative crystals obtained from the performed experiments**,** as a slight increase in crystal size is observed as the number of antisolvent injection points increases. Crystal shapes of prisms and needle-like forms were obtained; no significant differences in shape were observed between experiments.

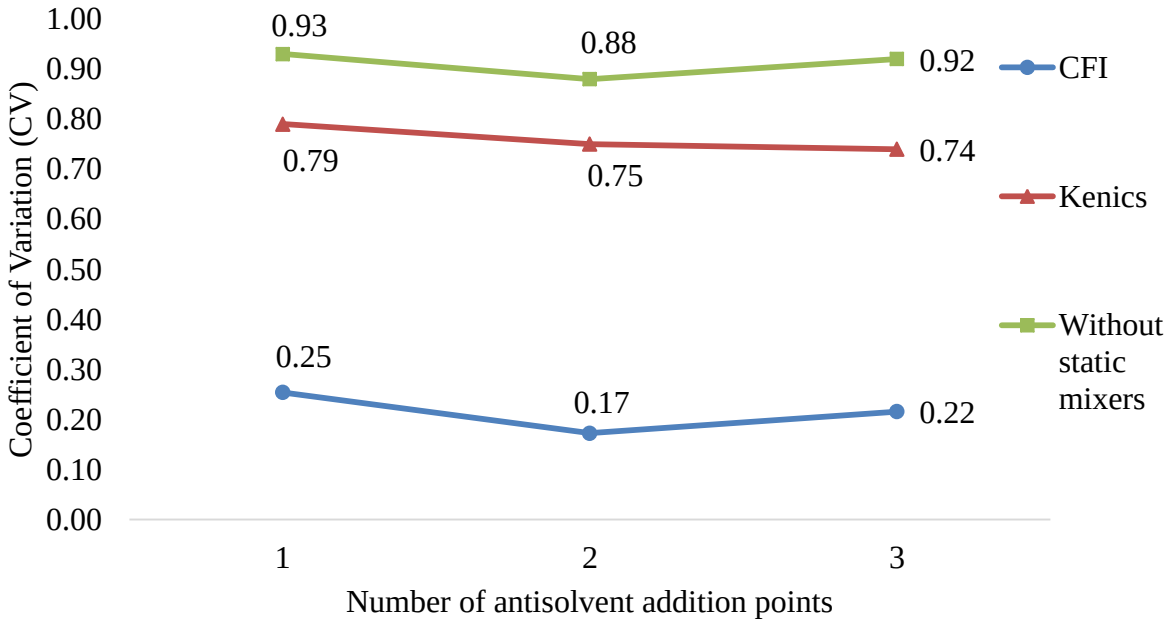

Figure 4.2. Effect of the use of Three Different Mixers in the Coefficient of Variation (CV) of Flufenamic Acid.

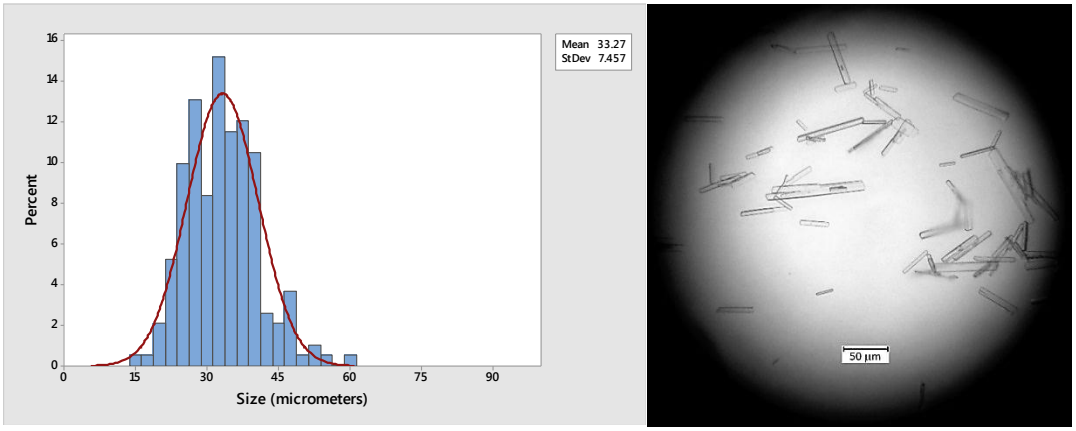

(a)

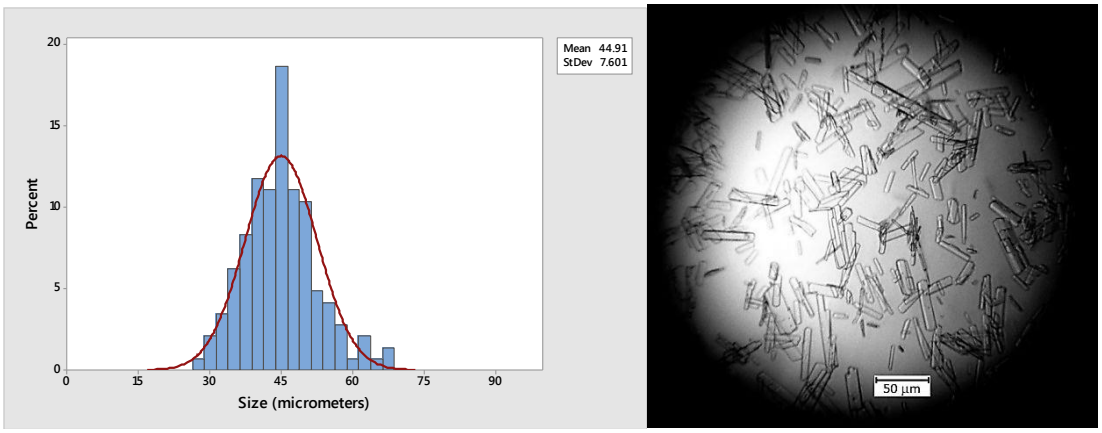

(b)

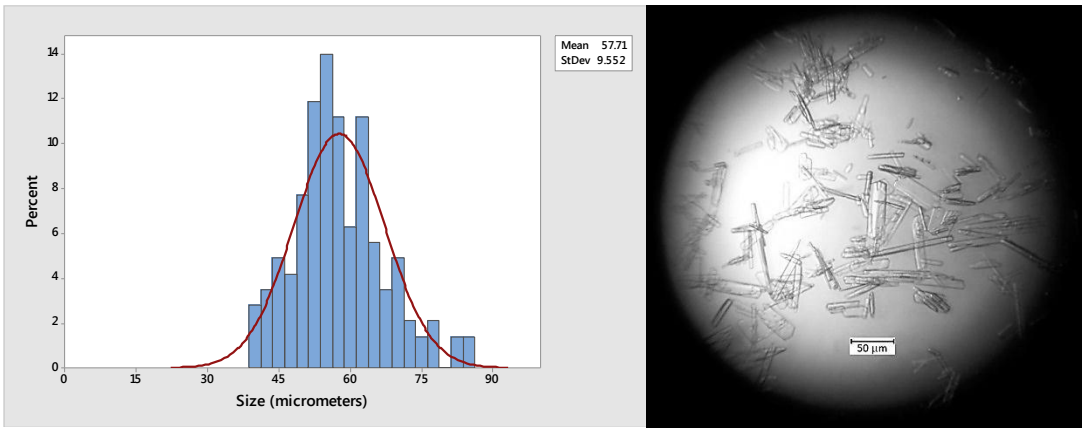

(c)

Figure 4.3. Crystal Size Distribution with corresponding Crystal Images for Flufenamic Acid with (a) One injection point (b) Two injection points (c) Three injection points

4.3 Effect of CFI's Configuration (varied number of 90-degree bends) on CSD in Antisolvent Crystallization Experiments

The effect of the number of 90-degree bends was evaluated on crystal size. The mean crystal size was 56.5, 45.5, 40.5 and 40.6 for a helical coil and CFIs with one, two, and three 90-degree bends, respectively. As can be seen in **Figure 4.4**, as the number of 90-degree bends increases, both mean crystal size and coefficient of variance decrease.

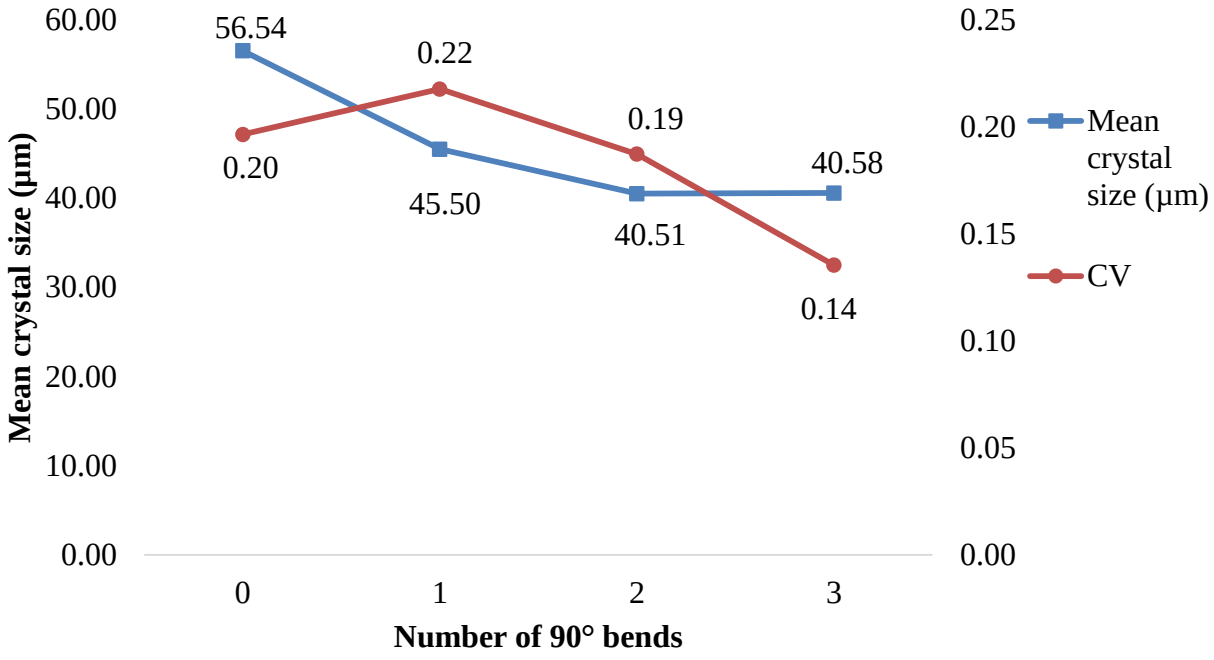

Figure 4.4. Effect of the Number of 90-degree bends on Mean Crystal Size

If a solution is not completely mixed before the crystallization starts, the crystallization proceeds under conditions of partial segregation, which would result in a wide crystal size distribution (Alvarez and Myerson, 2010). Thus, an effective homogeneous mixing that avoids the creation of uneven supersaturation conditions can explain the reduction in the coefficient of variance. As the number of 90-degree bends increases, a near plug flow is achieved. Consequently, near the reactor's entrance, crystals nucleate under the same supersaturation conditions, and as they move through the reactor, they grow under the same supersaturation conditions, thus resulting in a narrow CSD.

In the simulations of the Kenics type crystallizer implemented by Ridder et al. (2014) an increase in nucleation rates caused a decreased in CV since a smaller sized mode in the CSD was eliminated. In the experimental work by Nguyen et al. (2016) similar results were observed in a Couette-Taylor crystallizer. When the rotation speed was increased from 300 to 700 rpm, crystal size and coefficient of the size distribution gradually decreased from 87 to 82 μm and from 0.57-0.52, respectively.

Similarly, it has been reported that in oscillatory baffled crystallizers (COBC), an increase in oscillation amplitude or frequency enhances mixing intensity. This creates higher shear rates, which result in a higher dynamic nucleation rate with the production of smaller crystals. In the work by Brown et al. (2015), the antisolvent crystallization of salicylic acid in a COBC was studied. Contradictorily, when increasing the oscillatory Reynolds number (Re_o) from 1141 to 4562, a higher mean crystal size was obtained. This phenomenon was attributed to larger crystals that once became settled inside the crystallizer being brought into the suspension as the oscillation amplitude increased, resulting in a perceived increase in mean crystal size. This shows that when the intensity of the used mixing mechanism is increased, a narrow crystal size distribution is not necessarily obtained, as it may lead to particle deposit and resuspension. As this was not observed in the performed experiments, it can be concluded that increasing the number of 90-degree bends in a CFI is an effective method to obtain particles with uniform size.

In the work by Wiedmeyer, et al., (2017) crystallization in a helically coiled tube (HCT) was studied with Reynolds numbers equal to 1490, 1788, 20125, and 2550. For all Reynolds numbers a size-dependent crystal residence time was observed: larger crystals exhibited larger residence times than smaller crystals. This was attributed to smaller particles being affected by the secondary flow patterns formed in a HCT, thus taking longer paths than the larger crystals.

This behavior was hypothesized as a probable cause for obtaining a narrow CSD, since smaller crystals have more time to grow as they stay in the reactor for a longer time. However, since a CV of 0.14 was obtained for a CFI with three 90-degree bends, in comparison to a CV of 0.20 for a helical coil, it can be concluded that when Re = 500, flow inversion is a more important mechanism than size-dependent crystal residence time for obtaining a narrow CSD.

These results are in accordance with the experimental work by Klutz et al. (2015), in which the number of bends was the most significant factor in achieving a narrow RTD curve, when compared to inner tube diameter and Dean number. Additionally, according to equation (2.16), the parameter R_A takes values of 1, 0.5, 0.33, and 0.25 as the number of 90-degree bends increases from 0 to 3. The lower the value of R_A, the narrowest is the RTD; therefore, the lower CVs values are consistent with the expected results.

The experimental crystal size distribution of flufenamic acid for different number of 90-degree bends is presented in **Figure 4.5**.The presented graphs were obtained from image analysis of a set of twelve pictures taken from each experimental run using an optical microscope (Omax Professional Plan Laboratory Trinocular Compound Microscope) used with a 20x magnification. The graphs of **Figure 4.5** show a narrower crystal size distribution and a clear tendency of the graphs moving towards a smaller mean crystal size as the number of 90-degree bends increases. The crystal images of **Figure 4.5** were selected as representative crystals obtained from the performed experiments**,** as a decrease in crystal size can be observed as the number of 90-degree bends increases.

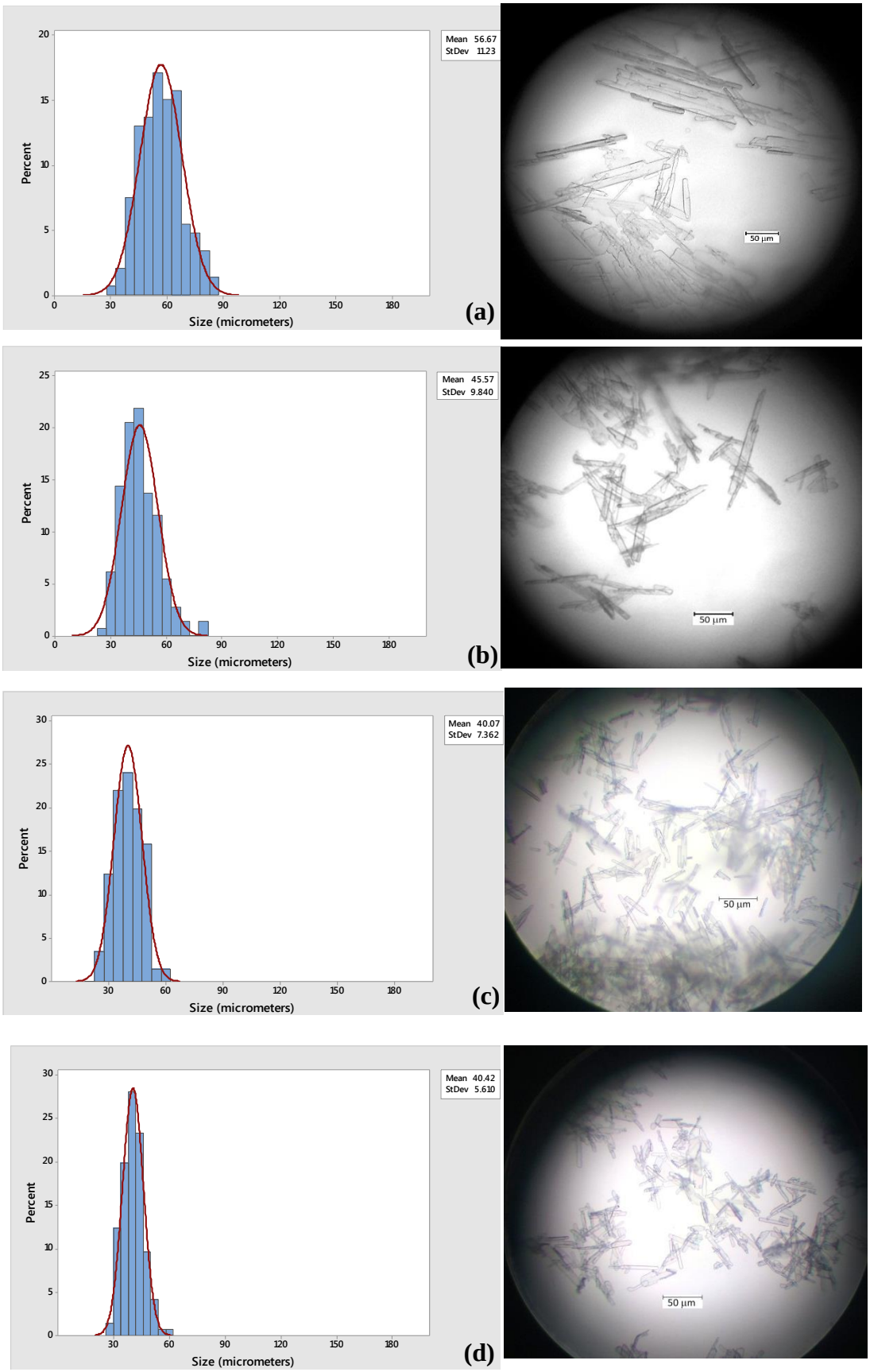

Figure 4.5. Crystal Size Distribution with corresponding Crystal Images for Flufenamic Acid for (a) Helical Coil (b) One 90° bend (c) Two 90° bends (d) Three 90° bends.

4.4 Comparison of Simulated and Experimental Results

The purpose of this section is to compare the numerical simulation results with the obtained experimental data. Mathematical modeling for antisolvent crystallization with one injection point, as well as for the helical coil reactor and CFIs with one, two, and three 90-degree bends was performed following the methodology described by Alvarez and Myerson (2010) and presented in section 2.3 of this thesis. The mathematical modeling of antisolvent crystallization with two and three antisolvent injection points is beyond the scope of this work and will not be included.

Estimated nucleation and crystal growth kinetic parameters and their confidence intervals for the continuous crystallization of flufenamic acid with one injection point, as well as for the helical coil reactor and CFIs with one, two, and three bends are presented in **Table 4.2**. The parameters were estimated for all experiments separately as stated by equation (2.9) using the steady-state crystal size distribution at the end of the CFI crystallizer.

Table 4.2. Estimated Nucleation and Crystal Growth Kinetic Parameters and 95% Confidence Intervals for Flufenamic Acid at One Antisolvent Addition Point and Different Number of 90° Bends

# addition points	k_g **(**$\times 10^{-5} m/s$)	G	k_b **(**$\times 10^{10} m/s$)	B
1	4.854 ± 1.55	1.0	8.639 ± 2.50	2.0
# 90 ° bends				
0	5.058 ± 0.15	1.0	1.136 ± 0.05	2.0
1	5.116 ± 0.10	1.0	2.628 ± 0.04	2.0
2	6.479 ± 0.14	1.0	5.502 ± 0.48	2.0
3	7.461 ± 0.06	1.0	6.767 ± 0.07	2.0

Table 4.2 shows that as the number of 90-degree bends increases, the nucleation rate constant (k_b) increased 495%, while the crystal growth rate constant (k_g) increased 48%, suggesting that nucleation is the most relevant process for these experiments.

Figure 4.6 shows a comparison of predicted and experimental crystal size distribution for flufenamic acid with one point of addition for the two performed experimental runs. A strong similarity between predicted and experimental values can be observed.

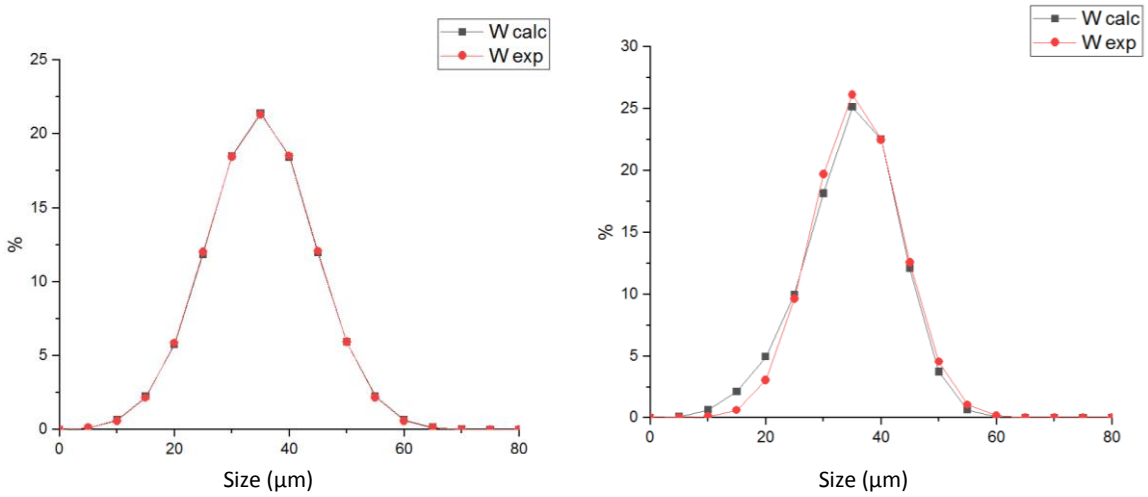

Figure 4.6. Comparison of Calculated and Experimental Crystal Size Distribution for Flufenamic Acid using the Plug Flow Model

In a similar matter, **Figure 4.7** shows a comparison of predicted and experimental crystal size distribution for flufenamic acid in a helical coil reactor (**Figure 4.7a**), CFI with one 90-degree bend (**Figure 4.7b**), with two 90-degree bends (**Figure 4.7c**), and with three 90-degree bends (**Figure 4.7d**). A strong fit can also be observed in all cases.

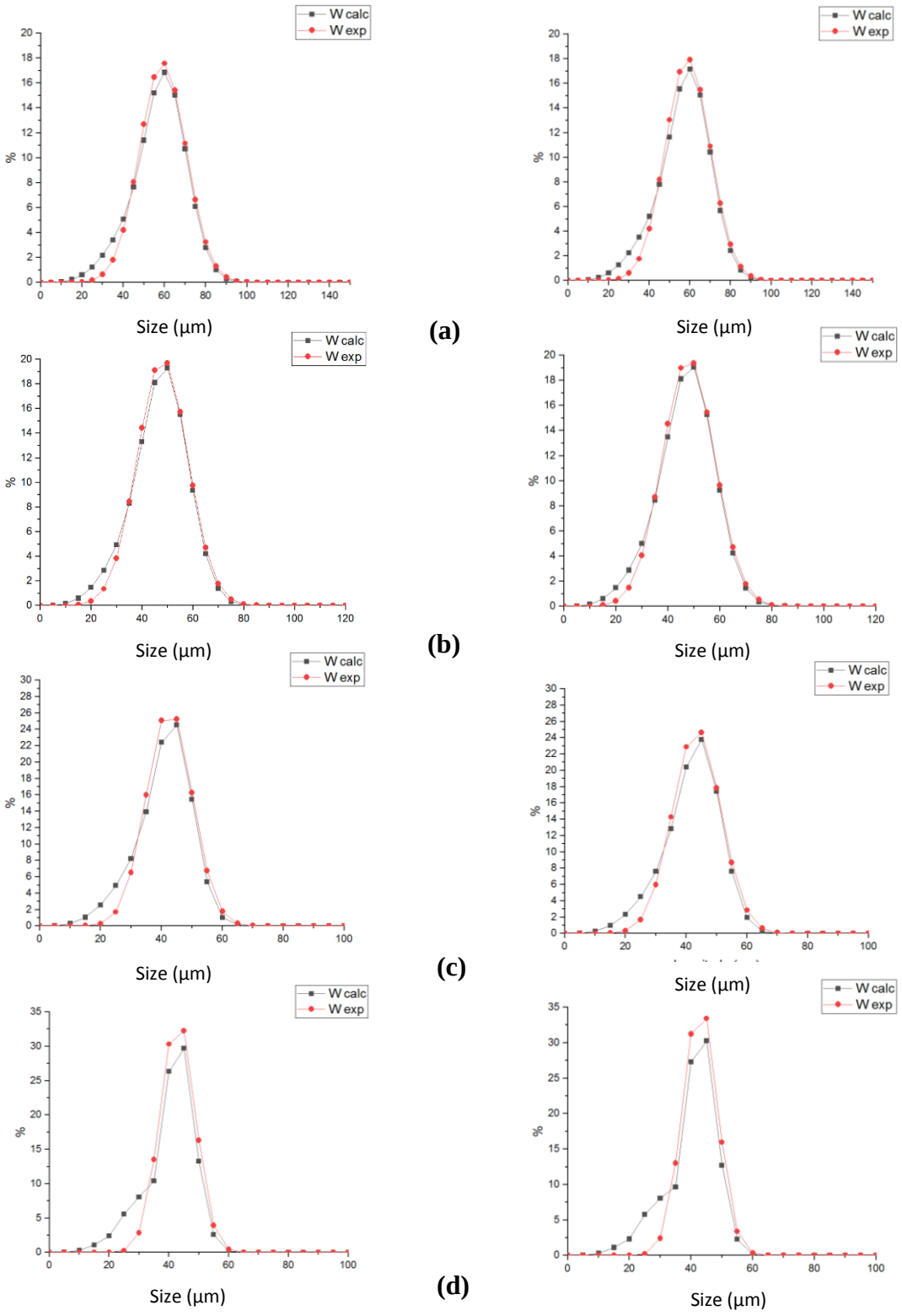

Figure 4.7. Comparison of Calculated and Experimental Crystal Size Distribution for Flufenamic Acid using the Plug Flow Model for
(a) Helical reactor (b) One 90° bend (c) Two 90° bends (d) Three 90° bends

In order to calculate the relationship between the estimated and experimental CSDs, W_{calc}, mass density as defined by equation (2.8) was plotted versus W_{exp}, which was the experimental mass density obtained. The regression coefficient between the two variables is presented in **Table 4.2**. **Figure 4.8** graphs W_{calc} versus W_{exp} including the corresponding fitting line for the two experimental runs of flufenamic acid crystallization using one antisolvent addition point.

Figure 4.9 graphs W_{calc} versus W_{exp} including the corresponding fitting line for the two experimental runs of flufenamic acid crystallization performed in a helical coil, and CFIs with one, two, and three 90-degree bends.

Table 4.3. Regression coefficient between Mass Density vs Experimental Mass Density for Flufenamic Acid

# addition points	**R^2**
1	0.9902
	0.9887
# 90 ° bends	**R^2**
0	0.9942
	0.9950
1	0.9818
	0.9848
2	0.9591
	0.9565
3	0.9999
	0.9940

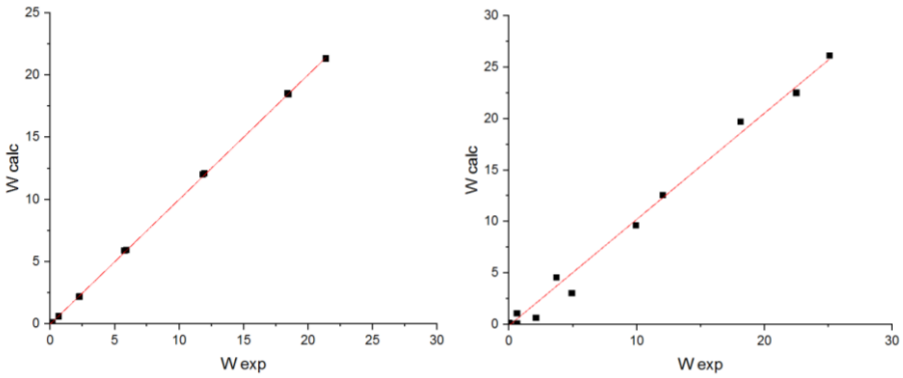

Figure 4.8. Calculated Mass Density vs Experimental Mass Density for Flufenamic Acid using One Antisolvent Addition Point

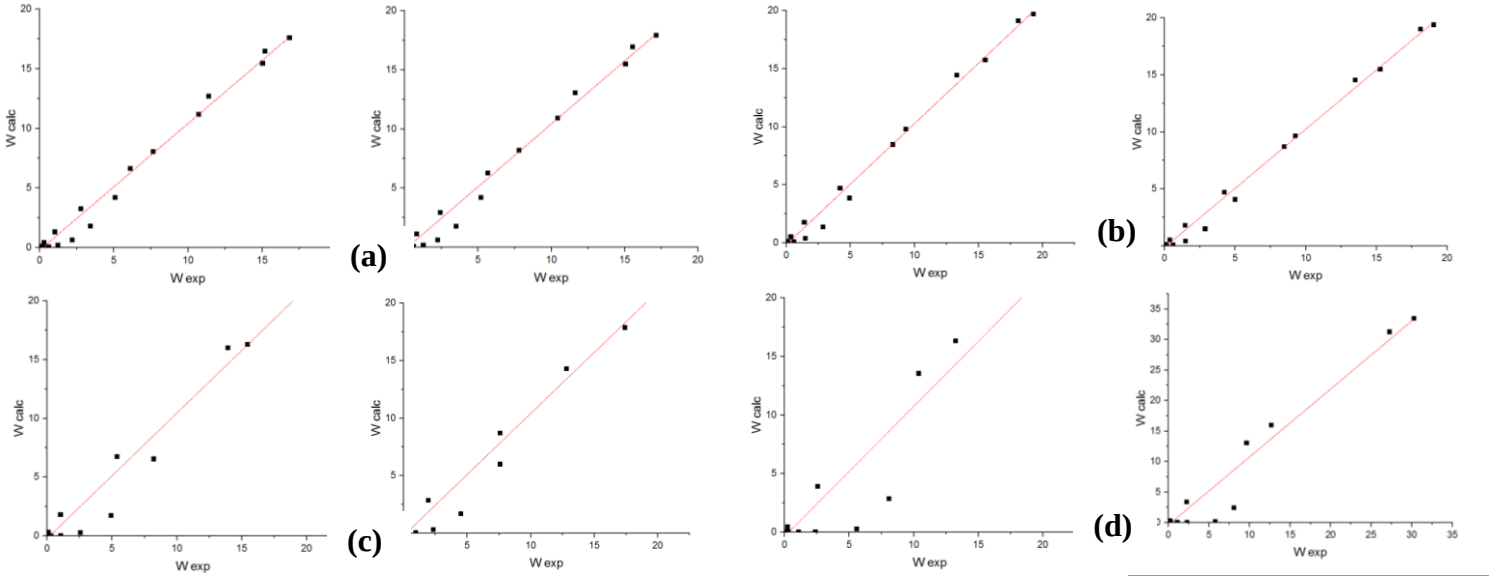

Figure 4.9. Calculated Mass Density vs Experimental Mass Density for Flufenamic Acid using (a) Helical Coil (b) One 90° bend (c) Two 90° bends (d) Four 90° bends

Growth rate dispersion (GRD) implies that crystals of the same size and shape grow at different rates in the same environment (Srisanga, et al., 2015). Random fluctuation of gowth rates can be caused by crystal collisions with each other and with mixing elements that result in changes in the dislocation network of crystals (Alvarez and Myerson, 2010). In the work by Hohmann et al. (2018) three population balance models were developed: size-independent growth only, size-independent growth that incorporates GRD, and size independent growth that incorporates both GRD and residence time distribution of the slurry. Of all three, the last model showed the highest regression coefficients (0.98) followed by the size-independent model. These results suggest that mean residence time of the crystals in the CFI is approximately equal to the overall mean residence time of the slurry. Nevertheless, different RTDs in the tubular crystallizer affect the CSD.

The population balance equation used in this work only incorporates size-independent growth, assumes no radial or axial dispersion, and no significant agglomeration, dissolution, or breakage. As a close fit was obtained between experimental and simulated results by this model (**Figures 4.8** and **4.9**), it can be concluded that near plug flow was achieved in the CFI crystallizer. Further tests may need to be performed in order to evaluate the effect of the RTD of crystals and slurry on CSD, however, the high values of R^2 (**Table 4.3**) suggest that it may not be a significant factor.

4.5 Evaluation of Process Intensification in terms of Mean crystal size, Coefficient of variation, and Pressure and Temperature Conditions

The intensification of a process has been defined as an improvement of its economic, environmental, health, and safety as well as operational aspects (Fernandez Rivas et al., 2018). In order to quantify and communicate to "outsiders" the drawbacks or benefits of a new technology, Fernandez Rivas et al. (2018) proposed a methodology that compares significant yet individual factors defined as *F*. For a given factor *F*, its value before modification F_b is divided by its value after modification, F_a. This ratio is then raised to an exponent *d*, whose absolute value indicates the importance of the factors with respect to the final goals of the intensification strategy, while its sign indicates whether a decrease in *F* is desired (positive sign), or undesired (negative sign). Considering a given number of *n* changes, the following product calculates the intensification factor defined by this methodology:

$$IF = \prod_{i=1}^{n} \left(\frac{F_b}{F_a}\right)^{d_i} \tag{4.3}$$

In this study, mean crystal size (μm) and coefficient of variation (CV) were considered as product quality indicators. According to Tsai et al. (2018), a drug's increased bioavailability can be achieved through a reduced particle size. Additionally, crystal size has been positively correlated to crystal defect density (number of defects per unit area) since larger crystals have a higher growth rate and thus less time for crystal lattice correction. Crystal defects alter the physicochemical and mechanical properties of the crystal as they act as high-energy sites that influence its chemical stability (Li, et al., 2010). On the other hand, crystal size distribution affects downstream operations and the physical and chemical properties of the final product as well. With this in mind, crystal engineering aims to minimize CSD variability (Besenhard et al., 2017). This study also considers crystallization and pre-expansion temperatures, as well as extraction pressure, as indicators of both energy savings and operational safety.

Table 4.4 presents the corresponding values of F_b for six different crystallization reactors/methods (batch, reactor without static mixers, Kenics type crystallizer, Kenics optimized, helical coil and RESS) used to crystallize flufenamic acid, which were compared to the F_a values obtained in the CFI experiments performed with three 90-degree bends (four

segments). These values were chosen as representative of the CFI's "best performance" due to the achieved reduction in particle size and variability. Since there is no information available of the relevance of each factor, the exponent *d* was set to unity in all cases. The sign of this exponent was defined as positive for all factors since as it has been beforehand mentioned, a decrease in mean crystal size and CV is desirable, while operation temperatures and pressures closer to ambient values translate into energy savings and a positive impact in safety.

Batch crystallization data was obtained from the experiments performed by Li et al. (2010) where flufenamic acid was dissolved in toluene at 65°C until supersaturation was reached. The solutions were allowed to cool down to room temperature with no agitation for eight hours, after which the crystals were collected. From an intensification point of view, the drawbacks of this system include a very high mean crystal size –probably from the lack of mixing- and an elevated operational temperature.

Crystallization data for the reactors without static mixers and the Kenics type mixer were obtained from the flufenamic acid crystallization experiments performed by Alvarez and Myerson (2010) with one antisolvent addition point. A significant improvement of the CV (0.93 vs. 0.79) and mean crystal sizes (93 vs. 67 µm) can be observed when the static mixers were added, however, the CFI was successful in creating a narrower CSD (CV=0.14) and crystals of smaller sizes (40.6µm).

Crystallization data for the Kenics optimized crystallizer was obtained from the simulations performed by Ridder at al. (2014). This theoretical investigation optimized the flowrates of antisolvent in the same crystallization set-up proposed by Alvarez and Myerson (2010) with the aim of reducing CV and increasing mass-mean crystal size. The values included in **Table 4.4** were the result of an optimal configuration of antisolvent flowrates as defined by the authors. From a process intensification perspective, the objective of comparing this work is to show that the CFI's experimental CSD is still narrower than an optimal simulated Kenics' CSD.

Crystallization data for the Rapid Expansion of Supercritical Solution (RESS) method was attained from the experiments performed by Tsai et al. (2018). The RESS technique allowed the preparation of ultra-fine particles of flufenamic acid through three main units: extraction, pre-

expansion, and precipitation. Although this method is effective in obtaining particles of very small sizes (2.62 μm), high operation pressures and temperatures are required.

Finally, the crystallization data presented for the helical coil was the same as described in section 4.3 of this thesis.

In this study, the exponent *d* was set with a value of one for all factors; however, the flexibility of the proposed process intensification evaluation method permits changing *d* in subsequent studies to indicate a higher or lower priority of energy savings and/or process safety over product quality.

Table 4.4 Calculation of Process Intensification in terms of Mean crystal size, Coefficient of variation, and Pressure and Temperature Conditions

	Crystallization reactor/method	Batch	W/o static mixers	Kenics	Kenics optimized	RESS	Helical coil	CFI	
				F_b				F_a	d
Factor	Mean crystal size (μm)	3200	93.0	67.0	92.0	2.62	56.54	40.58	1
	CV	0.21	0.93	0.79	0.21	0.37	0.20	0.14	1
	Extraction Pressure (MPa)	0.101	0.101	0.101	0.101	21	0.101	0.101	1
	Pre-expansion temperature (°C)	25	25	25	25	115	25	25	1
	Crystallization temperature (°C)	65	25	25	25	60	25	25	1
	IF_{total}	**307.54**	**15.22**	**9.32**	**3.40**	**392.56**	**2**	-	-

Due to the elevated pre-expansion pressure required for the RESS method, the total intensification factor for this crystallization reactor was the highest of all six (IF_{total} = 393). A high mean crystal size and crystallization temperature place the batch crystallizer in a second

place (IF_{total} = 308), while an elevated mean crystal size and CV place the crystallizer without static mixers in a third position (IF_{total} = 15). An improvement in variability and reduced mean crystal size is obtained in the Kenics (IF_{total} = 9) and the helical coil (IF_{total} = 2) crystallizers while operating at ambient conditions, yet the values of $IF_{total} > 1$ presented in **Table 4.4** indicate that the CFI with three 90-degree bends proved to be the most efficient –intensified- technology.

5. Conclusions and Future Work

In this work, the intensification of antisolvent continuous crystallization of an Active Pharmaceutical Ingredient (API) was investigated using the Coiled Flow Inverter (CFI) as a novel crystallization device. Two strategies were studied as means to control crystal size distribution (CSD) in the CFI technology: multistage antisolvent addition and a varied number of the reactor's 90-degree bends.

Mean crystal size of the studied API, flufenamic acid, increased with an increasing number of antisolvent addition points, thus suggesting a growth dominated process. On the other hand, mean crystal size decreased as the number of 90-degree bends increased, suggesting a nucleation dominated process. A narrower crystal size distribution (CSD) was also observed with an increased number of 90-degree bends. When compared to the CFI, mean crystal size and coefficient of variation were, in average, 1.8 and 3.5 times larger for the Kenics type crystallizer, respectively. This can be attributed to the high supersaturation induced by the effective mixing.

Using the Population Balance Equation, as a mathematical model to describe plug flow crystallization, crystal mass population density was calculated and compared with the obtained experimental data. High regression coefficients were obtained (0.96-0.99), which indicate that near plug flow behavior was achieved. Consequently, undesired crystallization process phenomena such as agglomeration, dissolution and breakage were successfully avoided, as they can lead to operational problems and a broad CSD.

The efficacy of the CFI can be attributed to the Dean vortices created by the action of unbalanced centrifugal forces that stabilize the flow. These vortices result in an improved radial mixing at laminar flow conditions, which is further enhanced with the addition of multiple flow inversions. This mechanism was successful in creating a high degree of homogeneity between the solution and the antisolvent, achieving a uniform supersaturation profile along the crystallizer, which results in controlled nucleation and crystal growth rates. The CFI system was also effective in creating a uniform suspension in which the mean residence time of the crystals in the CFIs is approximately equal to the overall mean residence time of the slurry.

The CFI technology provides the advantage of inducing chaotic advection at the 90-degree bends thus enhancing radial mixing without the use of moving parts, which results in reduced

operational costs as the only energy input is pumping. Moreover, this system is less complicated to fabricate and operate than other novel continuous crystallizers such as the sonicated tubular, Couette-Taylor, and the continuous oscillatory baffled crystallizer.

Process intensification (PI) was measured with the methodology proposed by Fernandez Rivas et al., 2018. Mean crystal size (μm) and coefficient of variation (CV) were considered as product quality indicators, while crystallization and pre-expansion temperatures, as well as extraction pressure, as both energy savings and operational safety indicators. Six crystallizers of flufenamic acid were compared (batch, reactor without static mixers, Kenics type crystallizer, Kenics optimized, helical coil and RESS) to a CFI with three 90-degree bends. The CFI was the most intensified technology of all six, with $\mathbf{IF_{total}}$ ranging from 2 (helical coil) to 392 (RESS). For this reason, it can be concluded that the main objective of this thesis, which was to intensify antisolvent crystallization processes, was achieved.

Since promising results were obtained for the fabricated CFI systems, future work may include studying the effect of different flow rates and/or residence times on the crystal size distribution. As it was mentioned in section 4.4, studying the RTD of the crystals and the slurry may be of interest to determine its effect on CSD. Cooling crystallization processes can also be explored as stainless-steel is a favorable heat conductor. The crystallization of different APIs or compounds used in the chemical or food industry can also be performed.

It would also be of interest to determine after how many 90-degree bends a considerable effect on crystal size distribution is no longer observed, since a very similar mean crystal size was observed in the experiments performed for CFIs with two and three 90-degree bends (~ 40.5μm) yet a reduced CV was obtained (0.19 and 0.14, respectively). This would require the fabrication of more CFI segments.

6. Bibliography

Ridder, B., Majumder, A., & Nagy, Z. (2014). Population Balance Model Based Multi-Objective Optimization and Robustness Analysis of a Continuous Plug Flow Antisolvent Crystallizer. *American Control Conference*, (pp. 3530-3535). Portland, Oregon, USA.

Alvarez, A. (2009). *Particle engineering through control of size and polymorphic forms of pharmaceutical products crystallized from solution. PhD Thesis.* Chicago, Illinois: Illinois Institute of Technology.

Alvarez, A., & Myerson, A. (2010). Continuous Plug Flow Crystallization of Pharmaceutical Compounds. *American Chemical Society*, 2219-2228 DOI:10.1021/cg901496s.

Babi, D., Sales Cruz, M., & Gani, R. (2016). Fundamentals of Process Intensification:A Process Systems Engineering View. DOI: 10.1007/978-3-319-28392-0_2.

Bassett, J.-M., & de Graaff, M. (n.d.). Continuous Helix Mini-Reactor . The Netherlands .

Behr, A., Brehme, V., Ewers, C., Grön, H., Kimmel, T., Küppers, S., et al. (2004). New Developments in Chemical Engineering for the Production of Drug Substances. *Engineering Life Science*, 15-24, DOI: 10.1002/elsc.200406127.

Besenhard, M., Neugebauer, P., Ho, C.-D., & Khinast, J. (2015). Crystal Size Control in a Continuous Tubular Crystallizer. *American Chemical Society*, 1683-1691 DOI: 10.1021/cg501637m.

Besenhard, M., Neugebauer, P., Scheibelhofer, O., & Khinast, J. (2017). Crystal Engineering in Continuous Plug-Flow Crystallizers. *American Chemical Society*, 6432-6444, DOI: 10.1021/acs.cgd.7b01096.

Brown, C., Adelakun, J., & Ni, X.-w. (2015). Characterization and modelling of antisolvet crystallization of salicylic acif in a continuous oscillatory baffled crystallizer. *Chemical Engineering and Processing*, 180-186 DOI:10.1016/j.cep.2015.04.012.

Cengel, Y., & Boles, M. (2015). *Thermodynamics: An Engineering Approach.* Mexico: McGrawHill.

Dortmund Data Bank. (n.d.). *Dynamic Viscosity of Ethanol*. Retrieved April 20, 2018, from http://www.ddbst.com/en/EED/PCP/VIS_C11.php

Drug Bank. (2018, March 08). *Flufenamic Acid*. Retrieved April 14, 2018, from https://www.drugbank.ca/drugs/DB02266

Extance, A. (2017, June 15). *Lilly pushes continuous drug production limits*. Retrieved April 14, 2018, from The Royal Society of Chemistry:

https://www.chemistryworld.com/news/lilly-pushes-continuous-drug-production-limits/3007584.article

Farmer, T. C. (2016). Polymorph selection by continuous crystallization. *AIChE* , 62: 3505–3514. doi:10.1002/aic.15343.

Fernandez Rivas, D., Castro-Hernández, E., Villanueva Perales, A., & van der Meer, W. (2018). Evaluation method for process intensification alternatives. *Chemical Engineering and Processing*, 221-232, DOI: 10.1016/j.cep.2017.08.013.

Fogler, H. (2006). *Elements of Chemical Reaction Engineering.* New Jersey: Prentice-Hall Inc.

Food and Drug Administration. (2017, September). *Advancement of Emerging Technology Applications for Pharmaceutical Innovation and Modernization Guidance for Industry*. Retrieved April 14, 2018, from https://www.fda.gov/downloads/Drugs/GuidanceComplianceRegulatoryInformation/Guidances/UCM478821.pdf

Furuta, M. M. (2016). Continuous crystallization using a sonicated tubular system for controlling particle size in an API manufacturing process. *Chemical Engineering and Processing*,, 210-218. DOI: 10.1016/j.cep.2016.02.002.

Hessel, V., Löwe, H., & Schönfeld , F. (2005). Micromixers—a review on passive and active mixing principles. *Chemical Engineering Science*, 2479 – 2501 DOI:10.1016/j.ces.2004.11.033.

Hohmann, L., Gorny, R., Klaas, O., Wohlgemuth, K., & Kockmann, N. (2016). Design of a Continuous Tubular Cooling Crystallizer for Process Development on Lab-Scale. *Chemical Engineering Technology*, 1-14 DOI: 10.1002/ceat.201600072.

Hohmann, L., Greinert, T., Mierka, O., Turek, S., Schembecker, G., Bayraktar, E., et al. (2018). Analysis of Crystal Size Dispersion Effects in a Continuous Coiled Tubular Crystallizer: Experiments and Modeling. *American Chemical Society*, 1459–1473, DOI: 10.1021/acs.cgd.7b01383.

Jacqueline, R. F.-J. (2017). Antisolvent crystallization of a cardiotonic drug in ionic liquids: Effect of mixing on the crystal properties. . *Journal of Crystal Growth*, 29-34. DOI: 10.1016/j.jcrysgro.2016.12.

Jiang, M., Zhu, Z., Jimenez, E., Papageorgiou, C., Waetzig, J., Hardy, A., et al. (2014). Continuous-Flow Tubular Crystallization in Slugs Spontaneously Induced by Hydrodynamics. *American Chemical Society*, 851-860, DOI: 10.1021/cg401715e.

Jolliffe, H., & Gerogiorgis, D. (2016). Plantwide design and economic evaluation of two ContinuousPharmaceutical Manufacturing (CPM) cases: Ibuprofen andartemisinin.

Computers & Chemical Engineering, 269-288, DOI:10.1016/j.compchemeng.2016.04.005.

Klutz, S., Kutup, S., & Lobedann, M. (2015). Narrow residence time distribution in tubular reactor concept for Reynolds number range of 10-100. *Elsevier*, 22-33 DOI: 10.1016/j.cherd.2015.01.003.

Lee, S., Lee, C.-H., & Kim, W.-S. (2016). Anti-solver crystallization of L-threonine in Taylor crystallizers and MSMPR crystallizer: Effect of fluid dynamics on crystal size, shape, and recovery. *Elsevier*, 119-127 DOI: 10.10106/j.jcrysgro.2016.08.021.

Lee, S., O'Connor, T., Yang, X., Cruz, C., Chatterjee, S., Madurawe, R., et al. (2015). Modernizing Pharmaceutical Manufacturing: from Batch to Continuous Production. *Journal of Pharmaceutical Innovation*, 191-199, DOI: 10.1007/s12247-015-9215-8.

Li, H., Stowell, J., Morris, K., & Byrn, S. (2010). Crystal Quality and Physical Reactivity in the Case of Flufenamic Acid (FFA). *Journal of Pharmaceutical Sciences*, 3839-3848, DOI 10.1002/jps.22221.

Liu, W. J. (2015). Analytical technology aided optimization and scale-up of impinging jet mixer for reactive crystallization process. *AIChE Journal* , 503-517. doi: 10.1002/aic.14662.

Lonare, A., & Patel, S. (2013). Antisolvent Crystallization of Poorly Water Soluble Drugs. *Chemical Engineering and Applications*, 337-341, DOI: 10.7763/IJCEA.2013.V4.321.

López, E. (2017). Fundamentos de Ingeniería de Microprocesos: Deposición en Micro-canales [PowerPoint Slides].

López, E. (2017). *Process Intensification Technologies for Mass-Transfer Limited Reactions: Case of Study Biodiesel Production. PhD Thesis.* Monterrey, Mexico: Monterrey Institute of Higher Technology and Education.

López-Guajardo, E., Ortiz-Nadal, E., Montesinos-Castellanos, A., & Nigam, K. (2017). Coiled flow inverter as a novel alternative for the intensification of a liquid-liquid reaction. *Chemical Engineering Science*, 179-185, DOI: 10.1016/j.ces.2017.01.016.

Massey, S. (2016, May 5). *Making The Switch: Continuous Manufacturing vs. Batch Processing of Pharmaceuticals*. Retrieved April 14, 2018, from xtalks: https://xtalks.com/continuous-and-batch-manufacturing-pharmaceuticals/

McCabe, W., Smith, J., & Harriott, P. (2007). *Unit Operations of Chemical Engineering.* Mexico: McGraw-Hill.

Mridha, M., & Nigam, K. (2007). Coiled Flow Inverter as an inline mixer. *Chemical Engineering Science*, 1724-1732. DOI: 10.1016/j.ces.2007.10.028.

Mullin, J. W. (2001). *Crystallization.* Oxford: Butterworth-Heinemann,.

Murphy, B. (2016, April 5). *Eli Lilly and Company announces initial €35 million capital investment at Biopharmaceutical campus in Kinsale*. Retrieved April 14, 2018, from IDA Ireland : https://www.idaireland.com/newsroom/eli-lilly-and-company-ann

Myerson, A. S. (2002). *Handbook of Industrial Crystallization.* New York: Butterworth-Heinemann.

Nagy, Z., & Braatz, R. (2012). Advances and New Directions in Crystallization Control. *Elsevier*, 55.75 DOI:10.1146/annurev-chembioeng-062011-081043.

Nguyen, A. K. (2010). Taylor vortex effect on phase transformation of guanosine 5-monophosphate in drowning-out crystallization. *Industrial and Engineering Chemistry Research*, 4865-4872. doi: 10.1021/ie901932t.

Nguyen, A.-T., Yu, T., & Kim, W.-S. (2012). Multiple Feeding Strategy for Phase Transformation of GMP in Continuous Couette−Taylor Crystallizer. *American Chemical Society*, 2780−2788 DOI: dx.doi.org/10.1021/cg201361e .

Nguyen, A.-T., Yu, T., & Kim, W.-S. (2016). Couette-Taylor crystallizer: Effective control of crystal size distribution and recovery of L-lysine in cooling crystallization. *Journal of Crystal Growth*, 65-77, DOI: 10.1016/j.jcrysgro.2016.10.020.

Ramkrishna, D., & Mahoney, A. W. (2002). Population balance modeling. Promise for the future. *Chemical Engineering Science*, 595 – 606, DOI:10.1016/S0009-2509(01)00386-4.

Rohani, S., & Omar, H. (2017). Crystal Population Balance Formulation and Solution Methods: A Review. *American Chemical Society*, 4028–4041, DOI:10.1021/acs.cgd.7b00645.

S. Karthika, T. K. (2016). A Review of Classical and Nonclassical Nucleation Theories. *American Chemical Society*, 6663-6681, DOI:10.1021/acs.cgd.6b00794.

Saxena, A. K., & Nigam, K. D. (1984). Coiled Configuration for Flow Inversion and Its Effect on Residence Time Distribution. *AIChE Journal*, 363-368 DOI:10.1002/aic.690300303.

Saxena, A., & Nigam, K. (1983). The effect of coil pitch and the cross-sectional ellipticity on RTD for diffusion-free laminar flow in helically coiled tubes . *Chemical Engineering Communications, ,* 277-289. DOI: 10.1080/00986448308940479.

Schaber, S., Gerogiorgis, D., Ramachandran, R., Evans, J., Bartoon, P., & Trout, B. (2011). Economic Analysis of Integrated Continuous and Batch Pharmaceutical Manufacturing: A Case Study. *American Chemical Society*, 10083-10092, DOI: 10.1021/ie2006752.

Srisanga, S., Flood, A., Galbraith, S., Rugmai, S., Soontaranon, S., & Ulrich, J. (2015). Crystal Growth Rate Dispersion versus Size-Dependent Crystal Growth: Appropriate Modeling for Crystallization Processes. *American Chemical Society*, 2330-2336, DOI:10.1021/acs.cgd.5b00126.

Thakur, R., Vial, C., Nigam, K., Nauman, E., & Djelveh, G. (2003). Static Mixers in the Process Industries- A Review. *Institution of Chemical Engineers*, 787-826 DOI: 10.1205/026387603322302968.

Tsai, C.-C., Lee, M.-J., & Ho-mu, L. (2018). Micronization of Flufenamic Acid with Rapid Expansion of Supercritical Solution (RESS) Method.

Vashisth, S., & Nigam, K. (2009). Prediction of flow profiles and interfacial phenomena for two-phase flow in coiled tubes. *Chemical Engineering and Processing*, 452–463, DOI: 10.1016/j.cep.2008.06.006.

W. R. Dean, M. A. (1928). Fluid motion in a curved channel. *Royal Society of London Mathematical, Physical, and Engineering Sciences*, 402-420, DOI: 10.1098/rspa.1928.0205.

Wang, T., Lu, H., Wang, J., Xiao, Y., Zhou, Y., Bao, Y., et al. (2017). Recent progress of continuous crystallization. *Journal of Industrial and Engineering Chemistry*, 14-29 DOI:10.1016/j.jiec.2017.06.009.

Wiedmeyer, V., Anker, F., Bartsch, C., Voigt, A., John, V., & Sundmacher, K. (2017). Continuous Crystallization in a Helically Coiled Flow Tube: Analysis of Flow Field, Residence Time Behavior, and Crystal Growth. *American Chemical Society*, 3699-3712, DOI:10.1021/acs.iecr.6b04279.

Wiedmeyer, V., Voigt, A., & Sundmacher, K. (2017). Crystal Population Growth in a Continuous Helically Coiled Flow Tube Crystallizer. *Chemical Engineering Technology*, 1584-1590, DOI: 10.1002/ceat.201600530.

Yu, L. (2016, April 12). *Continuous Manufacturing Has a Strong Impact on Drug Quality*. Retrieved April 14, 2018, from FDA Voice: https://blogs.fda.gov/fdavoice/index.php/2016/04/continuous-manufacturing-has-a-strong-impact-on-drug-quality/

Appendix A. Reynolds number, x_{cut} diameter and d_p diameter calculated for the different CFI segments on Experiments with Multiple Addition Points

The effect of multiple addition points of antisolvent on crystal size distribution was studied. In experiments with one injection point, 100 % (50 mL/min) of the antisolvent is injected at point 1. In experiments with two injection points, 50% (25 mL/min) of the antisolvent is injected at point 1 and 50% at point 2. In the case of three injection points, one third (16.67 mL/min) of the antisolvent is injected at points 1, 2, and 3.

As a result, the mass flow rate $\dot{m}$ decreased in the CFI segments, resulting in lower Reynolds numbers, smaller x_{cut} diameter as defined by equation 4.1, and higher particle diameter d_p as defined by equation 4.2. **Table A.1** presents these calculations for each of the CFI segments. CFI segment number 4 is not included since values remained constant for all experiments.

Table A.1 Effect of the Number of Antisolvent Addition Points on Reynolds number, x_{cut} diameter, and d_p diameter

Antisolvent addition points	**1**	**2**		**3**		
	CFI Segments					
Parameter	**1, 2, 3**	**1**	**2, 3**	**1**	**2**	**3**
Re	518.6	345.8	518.6	288.1	403.4	518.6
x_{cut}	731.9	597.6	731.9	545.5	645.5	731.9
d_p	125.0	153.1	125.0	167.7	141.7	125.0

Appendix B. Mean Crystal Size (Volume Based) for L-Glutamic Acid as a function of the Total Flow rate

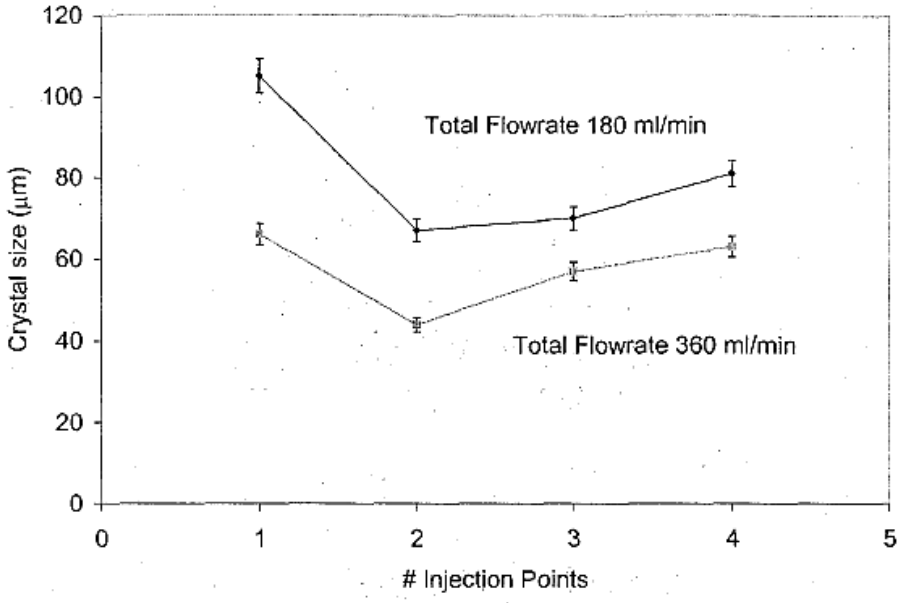

Figure B.1. Mean Crystal Size (Volume Based) for L-Glutamic Acid as a function of the Total Flow rate (Alvarez, 2009).